JOURNAL OF GEOPHYSICAL RESEARCH, VOL. 116, A08206, doi:10.1029/2010JA015667, 2011

Entropy distribution in the plasma sheet

Richard L. Kaufmann[1] and William R. Paterson[2]

Received 12 May 2010; revised 6 May 2011; accepted 13 May 2011; published 3 August 2011.

[1] Geotail data were used to study the long-term averaged spatial and flow speed dependencies of the ion entropy per unit volume and per unit flux tube and the average entropy per ion. It was concluded that some process associated with the production of fast flows substantially increased the entropy of an average ion. Entropy in the fastest flows exhibited little y dependence, showing that the process generating these flows near midnight was similar to the process acting near the flanks. It also was found that the irreversible aspect of reconnection does not change the entropy per ion significantly when two closed flux tubes are involved but can be significant during reconnection at the magnetopause or of two lobe flux tubes. The entropy per unit flux tube and $PV^{5/3}$ were compared. Both of these parameters provided useful information when there were gradients in the flux tube particle content. The difference between the average observed entropy per ion and the value that would be expected if the single particle distribution function $f(\mathbf{v})$ had evolved to an equilibrium Maxwellian was evaluated. After examining the effects of a non-Maxwellian equilibrium and of a generalized entropy, it was concluded that most of the observed deviation from standard equilibrium thermodynamics was produced by statistical fluctuations in the number of ion counts within the energy angle boxes used to evaluate $f(\mathbf{v})$ and that the remainder was attributable primarily to real plasma fluctuations.

Citation: Kaufmann, R. L., and W. R. Paterson (2011), Entropy distribution in the plasma sheet, *J. Geophys. Res.*, *116*, A08206, doi:10.1029/2010JA015667.

1. Introduction

[2] The goals of this work were to combine the spatial and flow speed dependencies seen in long-term averaged plasma sheet observations, to examine the relationships between several entropy parameters, to extend our previous analysis of the deviation from standard thermodynamics or the Boltzmann equilibrium of the average observed single particle velocity space distribution function, to determine whether any effects of irreversible processes can be detected, and to address questions concerning the use of Boltzmann thermodynamics in the plasma sheet.

[3] Entropy has been used as a measure of the capacity of a system to do work, e.g., in the Carnot cycle, of the probability of finding a closed system in a specific microscopic state, and of the complexity of a system. Spatial variations show where heat typically was deposited into or removed from a region of interest. Heat absorbed in or radiated from the plasma sheet could have propagated as waves from or to the dayside magnetopause, low latitude boundary layer (LLBL), plasma sheet boundary layer (PSBL), or ionosphere. The entry into or loss of particles from plasma sheet flux tubes at their ionospheric ends, the drift of particles through their sides, and particles that are lost during tail reconnection also change the average entropy per particle, per unit volume and per unit flux tube. Heat can be generated by shocks or the turbulent dissipation of nonthermal energy such as bulk flow energy. The thermalization of a mixture of hot and cold plasmas, the mixing of low- and high-density plasmas and the mixing of plasmas with different compositions are examples of irreversible processes that increase the average entropy per ion.

[4] *Kaufmann and Paterson* [2009, hereinafter paper 1] used Boltzmann's H-function with the normalization that was used by *Huang* [1963],

$$H_a(\mathbf{x},t) = \int f_a(\mathbf{x},\mathbf{v},t)\ln[f_a(\mathbf{x},\mathbf{v},t)]d^3v, \qquad (1)$$

to determine the long-term averaged spatial distribution of entropy, where $f_a(\mathbf{x}, \mathbf{v}, t)$ is the single particle velocity distribution function. The subscript a is i for ions, which were assumed to be protons, and e for electrons. The notation used here and the definitions of fluid parameters other than those involving $H_a(\mathbf{x}, t)$ are those used by *Rossi and Olbert* [1970]. Boltzmann used H to statistically define the entropy density of a gas that is not necessarily at equilibrium. His transport equation then was used to prove the H-theorem, which is a kinetic theory statement of the second law of thermodynamics for the evolution, through collisions, of non-

[1]Department of Physics, University of New Hampshire, Durham, New Hampshire, USA.
[2]Department of Atmospheric and Planetary Sciences, Hampton University, Hampton, Virginia, USA.

0148-0227/11/2010JA015667

equilibrium gases. The H-theorem shows that the Maxwell-Boltzmann distribution is the equilibrium state that connects Boltzmann's kinetic and the classical thermodynamic definitions of entropy.

[5] Paper 1 showed that the absolute magnitudes of spatial changes in the electron entropy were nearly the same as changes in the ion entropy within the plasma sheet. This similarity was attributed to the observation that the temperature ratio, T_i/T_e, near the neutral sheet, where $B_x = 0$, exhibited only weak spatial variations in the region studied [*Kaufmann et al.*, 2005, Figure 9]. Ion entropy is emphasized here because the measurements were not accurate enough to produce reliable plots of the average entropy per electron or of the deviation of electrons from thermodynamic equilibrium.

[6] Because of the logarithmic term, the value of $H_a(\mathbf{x}, t)$ has an intrinsic dependence on the units used and on the normalization of $f_a(\mathbf{x}, \mathbf{v}, t)$. For example, using all variables in MKS units does not produce H_a that is exactly 10^6 times the value of H_a obtained using all variables in cgs units. Paper 1 and the present study used MKS units and the same normalization, so direct comparisons of all parameters used here and in paper 1 can be made.

[7] All available 1 min averaged data from 10 years of Geotail magnetometer [*Kokubun et al.*, 1994] and Comprehensive Plasma Instrumentation (CPI) [*Frank et al.*, 1994] measurements were combined in paper 1 to create a single long-term averaged 3-D databased model of the $-30 < x < -8$ R_E, $-15 < y < 15$ R_E, $0 < |z| < 5$ R_E region. GSM coordinates aberrated by 4.5° were used. This model provided information about the spatial variations of many ion, electron and magnetic field parameters. The present study extends the investigation in paper 1 by using a series of twelve models based on data that also were sorted according to a magnetic flux transport parameter ϕ_c that is defined and discussed in section 2.1. This addition of ϕ_c sorting was introduced because most of the net particle, magnetic field and energy transport has been attributed to the relatively brief periods of very fast flows, or during bursty bulk flow (BBF) events [*Baumjohann et al.*, 1990; *Angelopoulos et al.*, 1994].

[8] The Boltzmann or kinetic entropy per unit volume is [*Huang*, 1963]

$$s_{H,a}(\mathbf{x}, t) = -k\, H_a(\mathbf{x}, t), \tag{2}$$

where k is Boltzmann's constant. The subscript H is used to identify Boltzmann entropy parameters that were derived from $H_a(\mathbf{x}, t)$ and that therefore include nonequilibrium properties of $f_a(\mathbf{x}, \mathbf{v}, t)$. Paper 1 showed that spatial gradients of $s_{H,a}(\mathbf{x}, t)$ could primarily be attributed to similar gradients of the particle density

$$n_a(\mathbf{x}, t) = \int f_a(\mathbf{x}, \mathbf{v}, t) d^3v. \tag{3}$$

Equation (3) shows the normalization used here for $f_a(\mathbf{x}, \mathbf{v}, t)$.

[9] Measures of the entropy per unit flux tube are of special interest in studies of the plasma sheet. The average Boltzmann ion entropy per unit flux tube is approximately

$$S_{Hf,i}(\mathbf{x}) = -k\, H_i(\mathbf{x}) V_f(\mathbf{x}), \tag{4}$$

where $V_f(\mathbf{x})$ is the volume of a tube containing 1 Wb of magnetic flux that crosses the neutral sheet at $\mathbf{x}$. Notations such as $H_i(\mathbf{x})$ refer to 10 year averages $\langle H_i(\mathbf{x}, t)\rangle$. Calculating $V_f(\mathbf{x})$ required the use of empirical magnetic field models only between the edges of our modeling region and the ionosphere. Details of the procedure used are described by *Kaufmann and Paterson* [2006].

[10] The approximation that $H_a(\mathbf{x}, t)$ was uniform along flux tubes was used because our twelve magnetic field models are much less sophisticated than those developed by *Tsyganenko* [1989, 1995, 1996]. Our models were produced by simply averaging B_x, B_y and B_z in the same manner that was used for the fluid parameters. The resulting average $\mathbf{B}$ values were attributed to the centers of the boxes and used to trace out the field lines. It was necessary to average data in 6×6 R_E (x, y) boxes and ~1 R_E z boxes to get enough points to make realistic 3-D models. Figure 1 of *Kaufmann et al.* [2004a] shows a set of models based on 6 year averages.

[11] The advantage of using our set of twelve $\mathbf{B}$ models is that it permitted us to incorporate the observation that the magnetic field was dipolar during fast flows and highly stretched during slow flows. However, fluid parameters in our crude $\mathbf{B}$ models typically fluctuated up and down along field lines by 20–30% from the values at the neutral sheet. If the approximation in equation (4) had not been used these unrealistic fluctuations would have required particle trapping in confined regions along each field line. We previously found that although it is easy to find anisotropic 1 min averaged distribution functions, the long-term averages of both ions and electrons were surprisingly isotropic near the neutral sheet [*Kaufmann et al.*, 2004a, 2005]. The assumption of isotropy does not influence the evaluation of other entropy parameters used in this paper.

[12] A parameter that is closely related to $S_{Hf,i}(\mathbf{x})$ is $P_i(\mathbf{x})V_f^{5/3}(\mathbf{x})$ [*Erickson and Wolf*, 1980; *Wolf*, 1983; *Kaufmann et al.*, 2004b; *Birn et al.*, 2009; *Johnson and Wing*, 2009; *Wang et al.*, 2009; *Wolf et al.*, 2009]. These two entropy parameters would be conserved during slowly evolving adiabatic processes involving a fixed number of particles confined within a flux tube, and are compared in section 2.3.3.

[13] Paper 1 showed that gradients of $S_{Hf,i}(\mathbf{x})$ were strongly correlated with gradients of $N_f(\mathbf{x})$, the average number of ions in a unit flux tube that crossed the neutral sheet at $\mathbf{x}$. Both V_f and N_f refer to a single hemisphere. Since most of the variations of $s_{H,a}(\mathbf{x})$ and $S_{Hf,a}(\mathbf{x})$ simply could be attributed to the observation that there was more entropy per unit volume or per unit flux tube when there were more particles in a unit volume or a unit flux tube, two dimensionless parameters that did not depend on the varying particle numbers also were evaluated.

$$\left(\frac{S}{N\, c_v}\right)_{H,a} = \left\langle -\frac{2\, H_a(\mathbf{x}, t)}{3\, n_a(\mathbf{x}, t)} \right\rangle \tag{5}$$

is the average dimensionless Boltzmann entropy per particle as determined using the measured non-Maxwellian $f_a(\mathbf{x}, \mathbf{v}, t)$. The entropy-per-particle parameters in this study were made dimensionless by expressing them in units of $c_v = 3k/2$, the average constant volume specific heat per particle for a classical ideal monatomic gas.

[14] The related parameter

$$\left(\frac{S}{N\ c_v}\right)_{P,a} = \left\langle 1 + \ln\left[\frac{2\pi P_a(\mathbf{x},t)}{m_a n_a^{5/3}(\mathbf{x},t)}\right]\right\rangle = \left\langle 1 + \ln\left[\frac{2\pi k T_a(\mathbf{x},t)}{m_a n_a^{2/3}(\mathbf{x},t)}\right]\right\rangle \quad (6)$$

is the dimensionless average entropy per particle of mass m_a that would exist if $f_a(\mathbf{x}, \mathbf{v}, t)$ evolved to an isotropic Maxwellian with the observed pressure $P_a(\mathbf{x}, t)$ or temperature $T_a(\mathbf{x}, t)$ and density $n_a(\mathbf{x}, t)$. Equation (6) was derived directly from equation (5) because the integral in equation (1) can be evaluated analytically when $f_a(\mathbf{x}, \mathbf{v}, t)$ is an isotropic Maxwellian. The subscript P on an entropy parameter indicates that it is based on the assumption of an isotropic Maxwellian or the standard thermodynamic Boltzmann equilibrium $f_a(\mathbf{x}, \mathbf{v}, t)$. Instead of evaluating $H_a(\mathbf{x}, t)$, the use of $(S/Nc_v)_{P,a}$ requires the evaluation of both the plasma bulk velocity

$$\mathbf{U}_a(\mathbf{x},t) = \int \mathbf{v}\, f_a(\mathbf{x},\mathbf{v},t) d^3v / n_a(\mathbf{x},t) \quad (7)$$

and the pressure tensor

$$\mathsf{P}_a(\mathbf{x},t) = \int m_a[\mathbf{v} - \mathbf{U}_a(\mathbf{x},t)][\mathbf{v} - \mathbf{U}_a(\mathbf{x},t)] f_a(\mathbf{x},\mathbf{v},t) d^3v \quad (8)$$

The scalar pressure is $P_a = 1/3\ Tr[\mathsf{P}_a]$. Although the fluid parameters defined in equations (1), (3), (7), and (8) were evaluated using integrals involving $f_a(\mathbf{x}, \mathbf{v}, t)$, the temperature tensor was evaluated in the satellite data analysis program using

$$\mathsf{P}_a(\mathbf{x},t) = n_a(\mathbf{x},t)\ k\ \mathsf{T}_a(\mathbf{x},t). \quad (9)$$

[15] The scalar temperature is defined as $T_a = 1/3\ Tr[\mathsf{T}_a]$ for either a Maxwellian or non-Maxwellian plasma [*Rossi and Olbert*, 1970; *Krall and Trivelpiece*, 1973], giving $3/2\ kT_a = 1/2\ mv_{th,a}^2$ for a 3-D nonrelativistic system, where $1/2\ mv_{th,a}^2$ is the average thermal energy per particle of species a. As will be seen in section 3.2, for plasmas containing beams or other non-Maxwellian features it sometimes is preferable to represent the particles of one species as two or more fluids, each with its own temperature, density and bulk flow velocity. Equation (6) shows that $(S/Nc_v)_{P,a}$ varies only because of changes in $P_a/n_a^{5/3}$, the entropy-per-particle parameter that has been used in previous studies of the plasma sheet [*Huang et al.*, 1989; *Goertz and Baumjohann*, 1991; *Borovsky et al.*, 1998; *Kaufmann et al.*, 2005; *Birn et al.*, 2006].

[16] Evaluation of both $(S/Nc_v)_{H,a}$ and $(S/Nc_v)_{P,a}$ permitted comparisons of entropy parameters that were based on H_a with similar parameters based on P_a and n_a. For example,

$$s_{P,a} = 3k\ n_a (S/Nc_v)_{P,a}/2 \quad (10)$$

with equation (6) gives the entropy per unit volume in a plasma with the observed n_a, P_a and a Maxwellian $f_a(\mathbf{v})$ while

$$S_{Pf,a} = 3k\ n_a V_f (S/Nc_v)_{P,a}/2 \quad (11)$$

with equation (6) gives the approximate entropy per unit flux tube in this plasma. Equations (10) and (11) permit a comparison of the observations presented here and in paper 1 with results produced by MHD simulations and with data sets that contain only n and P rather than $f(\mathbf{v})$ or H.

[17] If a fixed number N_i of ions in an isolated box evolved through two-particle collisions toward equilibrium, then the H-theorem shows that $(S/Nc_v)_{H,i}$ would tend to increase toward a maximum value of $(S/Nc_v)_{P,i}$. As a result, the difference between these two parameters

$$\delta\left(\frac{S}{Nc_v}\right)_i = \left(\frac{S}{Nc_v}\right)_{P,i} - \left(\frac{S}{Nc_v}\right)_{H,i} \quad (12)$$

was evaluated to provide a measure of the velocity space deviation of the observed ions from equilibrium. Even though the plasma sheet does not evolve due to ordinary two particle collisions, $\delta(S/Nc_v)_i$ provides a measure of the difference of the entropy per ion in the observed plasma from that in a standard thermodynamic equilibrium plasma with the same P_i and n_i.

[18] Section 2 is based on the series of twelve models, each of which was generated using only data from a preselected range of ϕ_c. These models were used to produce figures showing the ϕ_c, x, and limited y dependencies of most commonly used entropy parameters. The figures show both where the entropy-related parameters changed most abruptly as well as how much periods of small and large flow velocities contributed to the observed gradients. Section 2 includes an analysis of why the similarities and the differences between the entropy per unit flux tube parameters $P_i V_f^{5/3}$, $S_{Hf,i}$ and $S_{Pf,i}$ arose. Uncertainties associated with the limited number of ion counts available to evaluate each $f_i(\mathbf{x}, \mathbf{v}, t)$ also were examined.

[19] Section 3 contains a study of the magnitude of $\delta(S/Nc_v)_i$ that would be produced by several commonly used distribution functions. Since $\delta(S/Nc_v)_i$ was found to depend significantly upon the count rate, simulations were carried out to separate the real from the instrumental and data processing contributions to $\delta(S/Nc_v)_i$. This part of the study provides information about the spatial and flow speed variations of the long-term averaged deviation of magnetotail plasma from standard thermodynamic equilibrium. Effects that may be attributed to the nearly collisionless aspect of space plasmas also are addressed in section 3.

[20] The average entropy per ion is often considered as a conserved parameter during reconnection. This is not true if irreversible processes are associated with reconnection. Such processes are discussed and the principal results of the paper are summarized in section 4 and Appendix A.

2. Models Sorted by ϕ_c

2.1. Sorting Techniques

[21] Ten-year averaged 3-D models of several hundred plasma and field parameters were generated using the methods described by *Kaufmann et al.* [2001, 2002, 2005]. The 1 min averaged data points from the northern and southern hemispheres were combined to reduce statistical uncertainties in the long term averages. Only $B_z > 0$ observations were retained in order to remove most measurements within plasmoids and flux ropes and therefore to

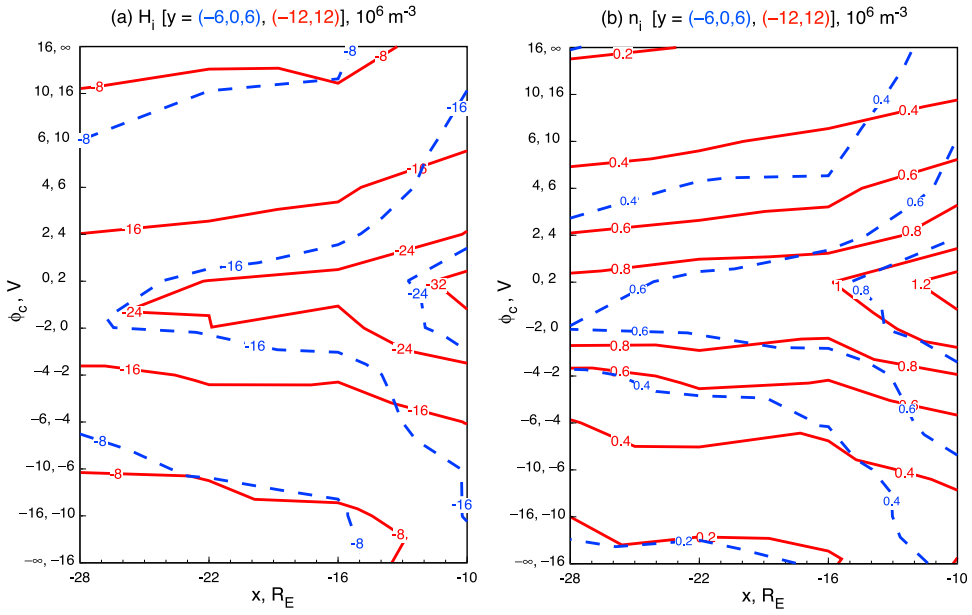

Figure 1. Contour plots showing the x and ϕ_c dependencies near midnight (blue dashed lines) and near the flanks (red solid lines) of the 10 year averaged (a) Boltzmann ion H-function and (b) ion density near the neutral sheet. The ordinate is labeled by the range of ϕ_c used to create each of the twelve 3-D models.

permit the integration needed to evaluate V_f. The data points were divided into twelve subsets according to a magnetic flux transport rate parameter ϕ_c. Data in each subset were sorted into 6 × 6 R_E (x, y) boxes. Data in each (x, y) box then were sorted into β_x boxes, where β_x is the ordinary plasma beta except that B_x was used instead of B to calculate the magnetic field pressure. The assumptions that β_x decreased monotonically when moving away from the neutral sheet and that the x component of the momentum equation was valid for long-term averages were used to calculate the z location of each β_x box edge [*Kaufmann et al.*, 2001]. Finally, linear interpolation in the z direction was used to evaluate each of the field and fluid parameters on a fixed (x, y, z) grid.

[22] The ϕ_c parameter was based on

$$E_c = \left[(U_{ix}B_z)^2 + (U_{iy}B_z)^2\right]^{1/2} \tag{13}$$

that was introduced by *Schödel et al.* [2001] for use in 2-D models as a measure of the magnetic flux transport rate. It was better to use E_c rather than U_i to define regions of fast flow because the average U_i in the region studied decreased substantially in the earthward direction while E_c had only a weak x dependence. Unusually fast flows therefore were identified more consistently as regions with E_c above a fixed E_{c0} than as regions of U_i above a fixed U_{i0}. Physically E_c is $|\mathbf{U} \times \mathbf{B}|$ at a point where $B_x = B_y = 0$. We sorted the data using ϕ_c, the maximum voltage drop across a unit flux tube with a locally circular cross section, to select the input data points needed to create each of the twelve 3-D models [*Kaufmann et al.*, 2005]. The radius of a circular tube containing 1 Wb of magnetic flux is $r_c = (\pi B)^{-1/2}$ so the perpendicular electric field $E_\perp = |\mathbf{U} \times \mathbf{B}|$ will produce a maximum voltage drop of $\phi_c = 2r_cE_\perp$. The assumption that $U_{iz} = 0$ was used when calculating ϕ_c because the Geotail spin axis was nearly in the z direction and measurements of the bulk flow speed along the spin axis were unreliable. However, all components of the measured **B** were included when calculating ϕ_c so the maximum voltage drop could be evaluated anywhere along a curved flux tube. It is the total bulk flow velocity that determines the magnitude of ϕ_c, not just the x component of the flow velocity. The sign convention was that $\phi_c > 0$ whenever the x component of $\mathbf{U}_i$ was positive. Even though cross-sectional shapes vary along flux tubes, ϕ_c remains more nearly constant than do other parameters that could easily be evaluated before the 3-D particle and magnetic field models were generated. Large $|\phi_c|$ was associated with large ion flow speeds, so large $|\phi_c|$ regions often will be referred to as fast flows. The explicit dependence of the average U_i on ϕ_c was shown using 8 year averaged models in Figure 1 of *Kaufmann et al.* [2005]. Nearly all the BBF measurements were contained in the data sets used to prepare the fastest flow models ($|\phi_c| > 16$ V).

2.2. Average Entropy Per Unit Volume

[23] Figure 1a shows the 10 year average of $H_i(x, y, \phi_c)$, and therefore of $s_{H,i}(x, y, \phi_c) = -k\,H_i(x, y, \phi_c)$. The use of 6 × 6 R_E (x, y) boxes gave y boxes centered at $y = -12$, -6, 0, 6 and 12 R_E. Although dawn-dusk asymmetries were present, most parameters showed similar structures in the region studied here in the two y boxes closest to the flanks ($y = \pm 12$ R_E) and similar structures in the three y boxes closest to midnight ($y = -6$, 0, 6 R_E). The plots only show averages of these groups of two or three y boxes rather than a separate curve for each y box. Figure 1 and most other plots were based on data from the z box closest to the neutral sheet ($|z| < 0.3$ R_E). Figures 1a and 1b extend the results in paper 1 by showing that the ϕ_c, x, and limited y dependencies of the plasma density n_i all were similar to those of $s_{H,i}$.

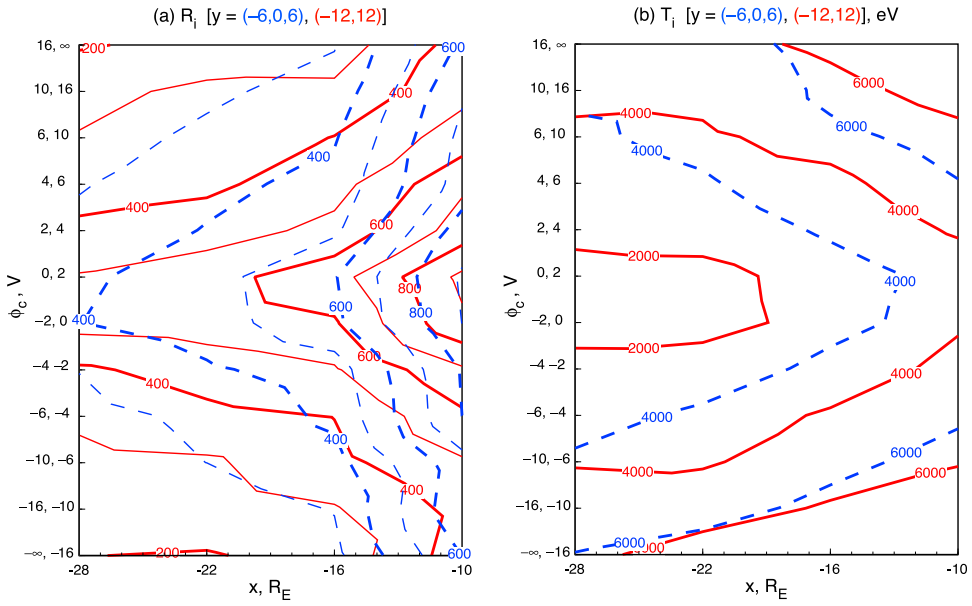

Figure 2. Similar to Figure 1 except showing (a) the ion count rate and (b) the ion temperature.

[24] The integrands in equations (1) and (3) depended upon $R_i(x, y, \phi_c)$, the average number of ion counts per minute (Figure 2a). The earthward increases of R_i, n_i and $s_{H,i}$ for all ϕ_c and for both y ranges were attributed primarily to the steep earthward decrease in V_f and the accompanying compression as plasma moved earthward. The decreases of R_i, n_i and $s_{H,i}$ as $|\phi_c|$ increased are consistent with the previously reported observation that plasma had a low density and a high temperature during BBF events [*Baumjohann et al.*, 1990; *Angelopoulos et al.*, 1994]. The low density during fast flows suggests that reconnection of the low density lobe flux tubes may be involved. However, any flux tubes containing hot plasma produced in association with reconnection events would tend to expand until the pressure was similar to that in neighboring slower flow flux tubes, also reducing the density. The ϕ_c dependencies of parameters examined in this paper were almost exclusively functions of the magnitude rather than the sign of ϕ_c. It was previously shown [*Kaufmann and Paterson*, 2006] that the net earthward transport of particle, magnetic field and energy fluxes in the region studied here occurred because fast earthward flow was more common than fast tailward flow and average earthward flow speeds were larger than average tailward flow speeds in the $|\phi_c| > 16$ V boxes.

[25] The most significant features in Figure 1 are that $s_{H,i}$ and n_i were larger at $x = -10$ R_E than at $x = -28$ R_E, larger near the flanks than near midnight, and larger in slow than in fast flows. The fastest flows exhibited similar particle and entropy densities regardless of whether they were seen near midnight or near the flanks. This feature also suggests that the generation of fast flows may have involved reconnection of field lines that initially extended into the far tail where large-scale y gradients tend to be small. The increases shown in paper 1 of $s_{H,i}(\mathbf{x})$ and $n_i(\mathbf{x})$ near the flanks now can be attributed primarily to observations made during periods of slow and moderate flow. The y gradient during such flows is consistent with the conclusion that sources of low temperature, high density and high entropy density plasma existed near the LLBL [*Sckopke et al.*, 1981; *Fujimoto et al.*, 1998; *Wang et al.*, 2006; *Nagata et al.*, 2008]. Once these relatively cold particles entered the magnetosphere they could diffuse toward midnight in response to the fluctuations in U_{iy} that were seen throughout the plasma sheet [*Johnson and Wing*, 2009; *Wang et al.*, 2010]. The senses of the x and y gradients and of the ϕ_c dependence of most parameters studied here are summarized in Table 1.

[26] Section 3 will show that the limited number of counts available when evaluating the 1 min averaged values of $f_i(\mathbf{x}, \mathbf{v}, t)$ introduced a substantial uncertainty in the determination of $\delta(S/Nc_v)_i$. No data points were used in this or our previous papers with ion count rates of $R_i < 80$. Justification

Table 1. Directions of the Gradients of the Plasma Parameters Analyzed Here[a]

	x	y	ϕ_c
$s_{H,i} = -kH_i$	E	f	S
n_i	E	f	S
T_i	E	m	F
P_i	E	m	W
V_f	T	f	W
N_f	T	f	S
$S_{Hf,i}$	T	f	S
$P_iV_f^{5/3}$	T	f	W
$T_iV_f^{2/3}$	T	W	F
$(S/Nc_v)_{H,i}$	E	m	F
$(S/Nc_v)_{P,i}$	W	m	F
$P_i/n_i^{5/3}$	W	m	F

[a]The top two parameters, $s_{H,i}$ and n_i, are quantities measured per unit volume. The next seven (T_i, P_i, V_f, N_f, $S_{Hf,i}$, $P_iV_f^{5/3}$, and $T_iV_f^{2/3}$) were used in studies of entropy per unit flux tube. The final three, $(S/Nc_v)_{H,i}$, $(S/Nc_v)_{P,i}$, and $P_i/n_i^{5/3}$, involve the average entropy per ion. For x gradients: E, earthward; T, tailward. For y gradients: f, toward the flanks; m, toward midnight. For ϕ_c gradients: S, toward slow flows; F, toward fast flows. For all parameters: W, weak.

for this cutoff is presented in section 3.3. Since Figure 2a shows that typical values of R_i near the neutral sheet were substantially larger than 80 counts per sample period, modest variations of the 80-count limit did not produce large changes in Figure 1. The sensitivity of fluid parameters to larger changes in the cutoff R_i was examined by sorting the data again to create five additional new sets of twelve models each using the same twelve ϕ_c ranges. Now, however, data were kept only if R_i exceeded 160, 320, 480, 640 and 800. Densities then were averaged over the five y boxes for each of the four x boxes, centered at $x = -28$, -22, -16 and -10 R_E. Changing the cutoff to $R_i = 160$ had almost no effect on $n_i(\mathbf{x})$ near the neutral sheet at $x = -10$ R_E and increased $n_i(\mathbf{x})$ by 11% at $x = -28$ R_E. Other fluid parameters used here, except for those involving the entropy per ion, changed by <10% when the cutoff R_i was increased to 160. As would be expected from Figures 1b and 2a, keeping only data points with $R_i > 800$ created average calculated $n_i(\mathbf{x})$ values several times larger than when an $R_i = 80$ cutoff was used. Nearly all the low-density data points had been removed, with the largest effects seen at $x = -28$ R_E.

2.3. Average Entropy Per Unit Flux Tube

[27] $S_{Hf,i}(\mathbf{x})$, $S_{Pf,i}(\mathbf{x})$ and $P_i(\mathbf{x})V_f^{5/3}(\mathbf{x})$ can be used to study variations of the average ion entropy per unit flux tube. Most thermodynamic theorems only apply to closed systems containing fixed groups of N particles. The relationship $PV^{5/3}$ = const. is typically used to characterize an adiabatic process in such a system containing a monatomic gas. The above three entropy parameters would be conserved during reversible adiabatic processes in the plasma sheet if all ions remained inside a flux tube. However, plasma sheet particles with different energies or charges drift at different velocities. It therefore is not possible to define a stationary or moving flux tube in the plasma sheet that is a closed system even if its open ionospheric ends are ignored. A flux tube could be considered as a nearly closed system if $\mathbf{U}_E = \mathbf{E} \times \mathbf{B}/B^2$ greatly exceeded other drift speeds. This seldom is true near the neutral sheet, where cross-tail drift velocities are high because the magnetic field line radius of curvature is less than a few Earth radii. Bounce-averaged cross-tail drift velocities are smaller than those near the neutral sheet. Figures 2 and 3 of *Larson and Kaufmann* [1996] illustrate these features of ion drifts associated with *Speiser* [1965] orbits in a thin current sheet. It therefore would appear that $P_iV_f^{5/3}$, $S_{Hf,i}$ and $S_{Pf,i}$ should all vary along average streamlines in long-term averaged models. However, simulations [*Birn et al.*, 2006, 2011] showed that although the entropy in the portion of a flux tube that remains connected to the ionosphere drops sharply during reconnection, the total entropy in this portion of a flux tube plus the entropy in the newly formed plasmoid is almost equal to the total entropy that existed in the flux tube before reconnection. This additive or "extensive" property of Boltzmann entropy and some reasons why alternative measures of entropy may be more suitable in space plasmas will be discussed in section 3.5. Sections 2.3.1–2.3.3 compare the entropy-per-unit-flux tube parameters that were defined in section 1. The basic variables that were used to evaluate these parameters also are examined to show how the observed gradients arose.

2.3.1. The x, y, and ϕ_c Dependencies of T_i, P_i, V_f, N_f, $P_iV_f^{5/3}$, and $T_iV_f^{2/3}$

[28] Figure 2b shows that the ion temperature near the neutral sheet exhibited an earthward increase at all ϕ_c and y. The sense of this x dependence was expected due to adiabatic compression as plasma moved to the unit flux tubes with smaller volumes that were found at lower altitudes. Little y dependence of T_i was evident when the bulk flow was fastest. Therefore the observation in paper 1 that T_i was lower near the flanks than near midnight can be attributed to slow and moderate flow periods. When combined with the lack of y dependence of n_i during the fastest flows, it is concluded that similar low densities and high temperatures are characteristic of fast flows and BBF events regardless of their y location. The strong ϕ_c dependence of T_i suggests that ions were heated during whatever process created the fast flows, or else that fast and slow flow plasmas came from entirely different sources.

[29] Figure 3a shows that $P_i = n_ikT_i$ increased in the earthward direction for all ϕ_c and y, as would be expected as a result of adiabatic compression. Both n_i and T_i had comparable earthward gradients to produce this earthward gradient of P_i. Pressure also is seen to be lower at the neutral sheet near the flanks than near midnight. The anticorrelation between n_i and T_i as a function of ϕ_c was strong enough to produce little consistent ϕ_c dependence of P_i. The lack of ϕ_c dependence can be understood as a consequence of the localization of fast flows [*Angelopoulos et al.*, 1996; *Sergeev et al.*, 1996]. If a localized fast flow region was generated with an unusually high or low P_i, the region would expand or contract until it had a pressure that was similar to that of the surrounding slower flow region.

[30] Figure 3b shows that V_f decreased when moving earthward and was larger near the flanks than near midnight. The strong earthward decrease of V_f was produced by both the earthward increase in B with the associated decrease in cross-sectional area of a unit flux tube and the earthward decrease in flux tube length. Only a weak dependence on ϕ_c is evident except possibly in the most distant, fastest flow regions. Our calculations of V_f were most uncertain in these distant fast flows because this is where field lines were most nearly dipolar. A large fraction of a distant strongly dipolar flux tube lies outside the $|z| < 5$ R_E region where our 3-D models can be used, so its calculated volume depends significantly upon the T89 [*Tsyganenko*, 1989] and dipole field models that were used to follow field lines from $|z| = 5$ R_E to the ionosphere. A discussion of why V_f depended only weakly on ϕ_c was included in work by *Kaufmann and Paterson* [2006].

[31] Since both P_i and V_f depended weakly on ϕ_c, it is not surprising that the average $P_iV_f^{5/3}$ also had a weak ϕ_c dependence (Figure 4a). The x and y gradients of $P_iV_f^{5/3}$ had the same sense as did the gradients of V_f, and were opposite to those of P_i. The observations that the long-term averaged earthward increase of P_i was smaller than would be expected from adiabatic compression if all ions remained in earthward moving flux tubes, and therefore that the average $P_iV_f^{5/3}$ exhibited an earthward decrease, were used to identify the pressure balance inconsistency (PBI) problem [*Erickson and Wolf*, 1980].

[32] Figure 4b shows that there was a strong earthward decrease of N_f in both y regions and at all ϕ_c. Although n_i

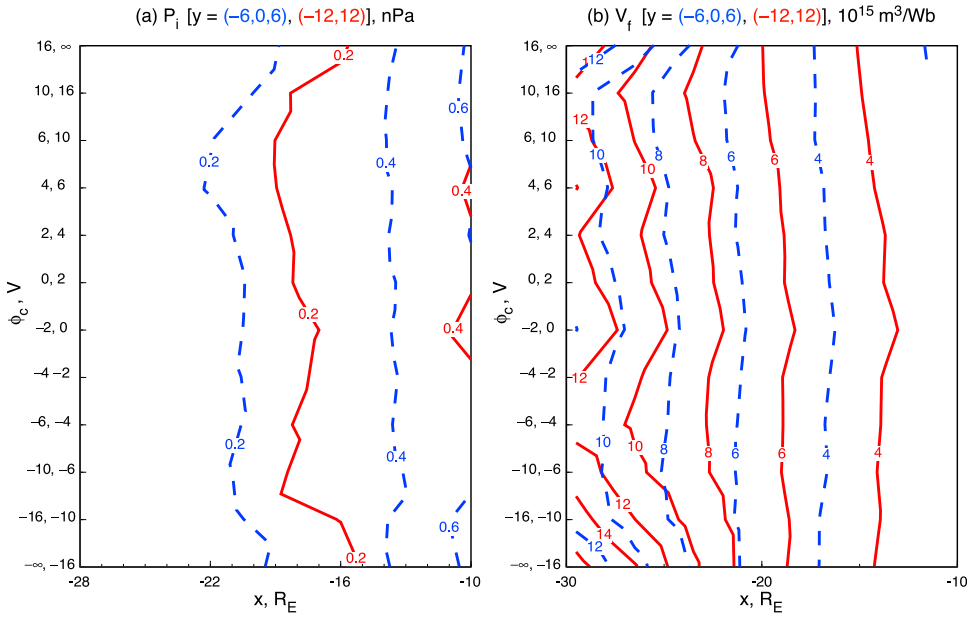

Figure 3. Similar to Figure 1 except showing (a) the ion pressure and (b) the volume, in one hemisphere, of a tube containing 1 Wb of magnetic flux.

exhibited an earthward increase (Figure 1b), V_f had a much steeper earthward decrease (Figure 3b). The resulting x gradient of N_f is closely associated with the PBI [*Erickson and Wolf*, 1980; *Borovsky et al.*, 1998; *Kaufmann and Paterson*, 2006; *Wang et al.*, 2009; *Lyons et al.*, 2009]. It also is seen that slow flow flux tubes contained many more particles than did fast flow flux tubes because V_f had a weak ϕ_c dependence while n_i was much smaller in fast than in slow flow regions (Figure 1b). Finally, Figure 4b shows that the average flux tube content was smaller near midnight than near the flanks, as was V_f (Figure 3b).

[33] Another parameter that has been used in entropy studies is the energy invariant $T_i V_f^{2/3}$, which is conserved in a flux tube if N_f and $P_i V_f^{5/3}$ are conserved and elastic pitch angle scattering maintains isotropy [*Wolf*, 1983]. These entropy studies assumed that particle groups originated at multiple source locations, each group being characterized by a different $T_i V_f^{2/3}$ and $f(\mathbf{v})$. The drift motions of many groups were followed back from a desired destination to their source locations and were then combined to determine the $f(\mathbf{v})$ expected at the destination [*Spence and Kivelson*, 1993; *Garner et al.*, 2003; *Wang et al.*, 2006, 2009; *Wolf et al.*,

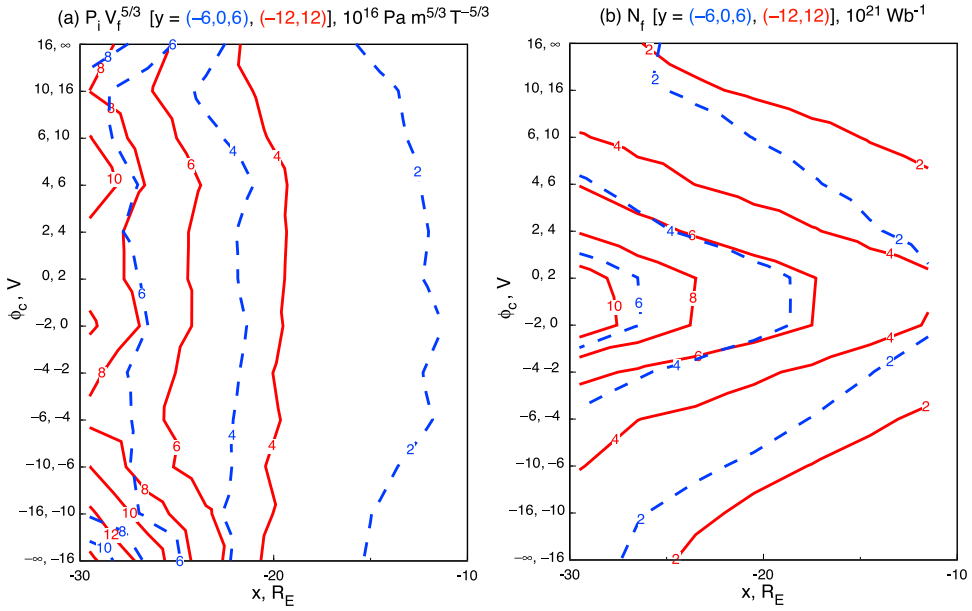

Figure 4. Similar to Figure 1 except showing (a) $P_i V_f^{5/3}$ and (b) the number of ions contained in one hemisphere of a unit flux tube.

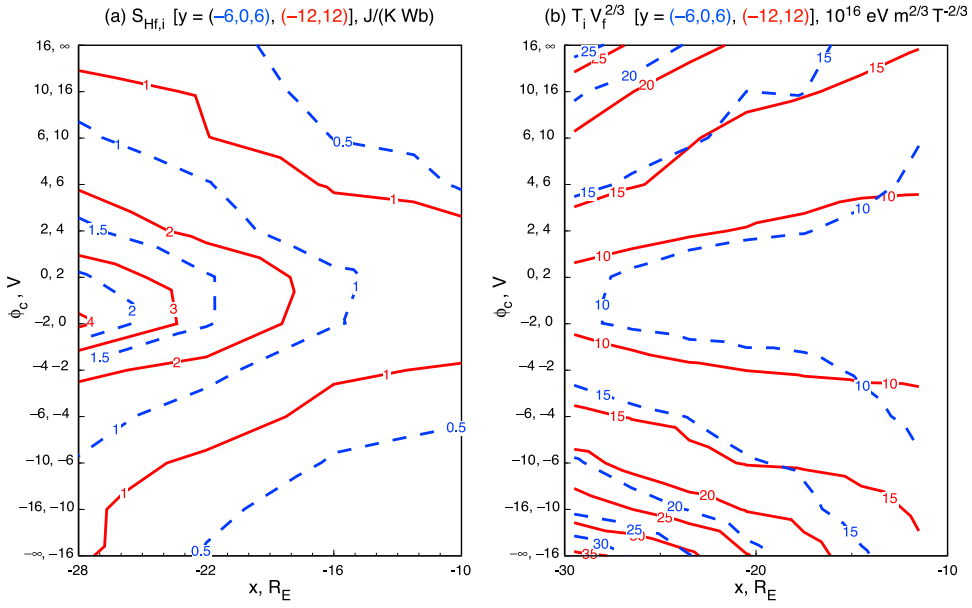

Figure 5. Similar to Figure 1 except showing (a) the total ion entropy in one hemisphere of a unit flux tube and (b) the ion energy invariant $T_i V_f^{2/3}$.

2009; *Zhang et al.*, 2009]. Figure 5b shows that the earthward decrease of $V_f^{2/3}$ dominated over the earthward increase of T_i. Combining $P_i = n_i k T_i$ and $N_f = n_i V_f$ gives

$$kT_i V_f^{2/3} = P_i \, V_f^{5/3} / N_f \tag{14}$$

so $kT_i V_f^{2/3}$ also is the average $P_i V_f^{5/3}$ per ion. A resulting important property of $T_i V_f^{2/3}$ is that it will be conserved in a flux tube if the only reason why $P_i V_f^{5/3}$ is not conserved is because $P_i V_f^{5/3}$ is linearly dependent on N_f. Both $P_i V_f^{5/3}$ and N_f had strong tailward x gradients but that of $P_i V_f^{5/3}$ was stronger, resulting in the relatively weak tailward gradient of the average $T_i V_f^{2/3}$. Both $P_i V_f^{5/3}$ and N_f were a little larger near the flanks than near midnight, resulting in little consistent y dependence of $T_i V_f^{2/3}$. With regard to correlations with the flow velocity, the long-term averaged $P_i V_f^{5/3}$ was seen to depend only weakly on ϕ_c. As a result, the ϕ_c dependence of $T_i V_f^{2/3}$ had a reciprocal relationship to that of N_f (Figure 4b). This again reflects the observation that fast flows typically involved high temperature but low density plasmas, suggesting that the generation of fast flows was associated with a strong heating process.

[34] To summarize the structure of this large group of parameters (see Table 1), T_i and P_i had earthward gradients but V_f had a steeper tailward gradient. As a result N_f, $P_i V_f^{5/3}$ and $T_i V_f^{2/3}$ also had tailward gradients. Earthward reductions of N_f and $P_i V_f^{5/3}$ were associated with the PBI. The y dependencies of these variables were characterized by increases of V_f, N_f and $P_i V_f^{5/3}$ along with decreases of T_i and P_i when moving from midnight to the flanks. There was little consistent y dependence of $T_i V_f^{2/3}$. Finally, T_i and $T_i V_f^{2/3}$ increased while N_f decreased as the flow velocity increased. Both P_i and V_f, and therefore $P_i V_f^{5/3}$, were only weakly dependent on ϕ_c.

2.3.2. The x, y, and ϕ_c Dependencies of $S_{Hf,i}$

[35] The combination of Figures 1a and 3b shows why $S_{Hf,i} = -kH_i V_f$ exhibited such a steep earthward decrease (Figure 5a). The fractional decrease of V_f between $x = -28$ R_E and $x = -10$ R_E substantially exceeded the fractional increase of $s_{H,i} = -kH_i$ in this same region. It may seem inconsistent to refer to the fractional change of $-kH_i$ because the absolute value of H_i depends on the units used. An absolute value of the entropy can be specified by the principle that it should approach zero as the temperature approaches zero, a feature that is referred to as the third law of thermodynamics. This requirement is not consistent with our assumption that the ions can be treated as a classical ideal monatomic gas with a constant heat capacity per ion of $c_v = 3k/2$ all the way to $T_i = 0$. The ideal gas assumptions are valid for high temperature, low density gases. Both entropy and heat capacity must approach zero as T_i approaches zero to be consistent with the third law. However, the entropy given by equation (6) passes through zero only when $T_i < 6 \times 10^{-6}$ eV if $n_i = 1$ cm^{-3} or when $n_i > 7 \times 10^7$ cm^{-3} even if T_i is as low as 1 eV. These extremely cold or very dense conditions are so remote from those of the typical plasma sheet that equations (4) and (6) appear to be adequate when examining the relationship between $S_{Hf,i}$ and $P_i V_f^{5/3}$.

[36] A possible explanation of the gradients of $S_{Hf,i}$ and N_f from midnight toward the flanks seen in Figures 4b and 5a (see also Figure 3a of paper 1 and *Kaufmann et al.* [2004b, Figure 2]) is that the average entropy per unit flux tube was affected by substorms. Both N_f and $S_{Hf,i}$ were smaller near midnight, where substorms were most common, than near the flanks. Reconnection during a substorm removes plasma and the associated entropy from a closed unit flux tube when a plasmoid or detached flux rope is formed. Another possibility is that the bubbles or fast flow flux tubes with low $S_{Hf,i}$ and N_f preferentially transport plasma toward midnight.

[37] Figure 5a shows that $S_{Hf,i}$ was substantially smaller in fast than in slow flow regions. This observation shows that when data from all ϕ_c were combined to make a single long-term averaged model (paper 1), the average entropy per unit flux tube was determined primarily by data from

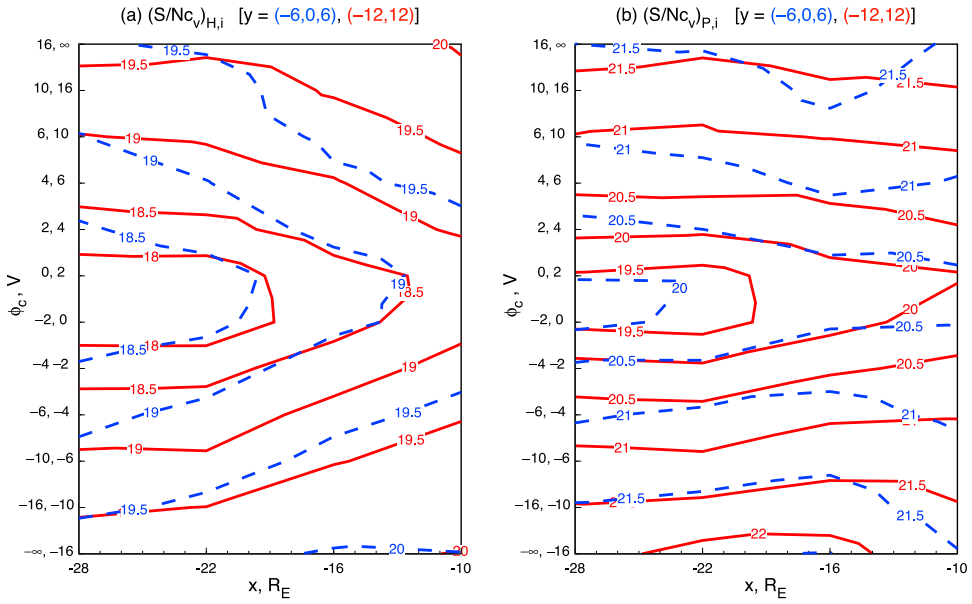

Figure 6. Similar to Figure 1 except showing (a) the average entropy per ion parameter $(S/Nc_v)_{H,i}$ in units of $c_v = 3k/2$ based on the measured $f(\mathbf{v})$ and (b) the equivalent average entropy per ion $(S/Nc_v)_{P,i}$ based on a Maxwellian with the measured P_i and n_i.

slow and moderate flow periods. The observation that the fast flow small $S_{Hf,i}$ regions, that are characterized by low densities and high temperatures, are most common near midnight also could be associated with the tendency for cold dense plasma to be seen most often near the flanks. However, the clearest features of the x, y and ϕ_c dependencies of $S_{Hf,i}$ near the neutral sheet are that they primarily reflect similar dependencies of N_f.

2.3.3. Relationships Between $P_iV_f^{5/3}$, $S_{Hf,i}$, and $S_{Pf,i}$

[38] The interpretation of long-term averaged data can be more confusing than is a typical thermodynamic study of a system containing a fixed number of particles. Section 2.3.3 was prepared to examine the complex relationships between $P_iV_f^{5/3}$ and either $S_{Hf,i}$ or $S_{Pf,i}$, all of which are related to the entropy in a unit flux tube. The average $P_iV_f^{5/3}$ can be compared quantitatively to the average $S_{Pf,i}$ when the isotropic Maxwellian assumption is adequate. Figure 6 shows that variations of $(S/Nc_v)_{H,i}$ and $(S/Nc_v)_{P,i}$, and therefore of $S_{Hf,i} = N_f(S/Nc_v)_{H,i}$ and $S_{Pf,i} = N_f(S/Nc_v)_{P,i}$, were similar with $S_{Pf,i}$ and $(S/Nc_v)_{P,i}$ generally ~10% larger than $S_{Hf,i}$ and $(S/Nc_v)_{H,i}$. The variations of $S_{Hf,i}$ and $S_{Pf,i}$ therefore will be considered nearly equal except when examining the deviation from standard thermodynamic equilibrium.

[39] Combining the ϕ_c-dependent version of equation (6) with the relations $n_i(\mathbf{x}, \phi_c) = N_f(\mathbf{x}, \phi_c)/V_f(\mathbf{x}, \phi_c)$ and $c_v = 3k/2$ gives

$$S_{Pf,i}(\mathbf{x},\phi_c) = \left(\frac{3k}{2}N_f(\mathbf{x},\phi_c)\right)\left[1+\ln\left(\frac{2\pi P_i(\mathbf{x},\phi_c)V_f^{5/3}(\mathbf{x},\phi_c)}{m_i N_f^{5/3}(\mathbf{x},\phi_c)}\right)\right]. \quad (15)$$

[40] Since equation (15) depends linearly upon N_f and only logarithmically on $P_iV_f^{5/3}$ and since $S_{Hf,i}$ (Figure 5a) and N_f (Figure 4b) are qualitatively similar, it might appear that $P_iV_f^{5/3}$ would be only weakly related to $S_{Pf,i}$ or $S_{Hf,i}$. However, sections 2.3.1 and 2.3.2 and Figures 4a and 5a showed that although the ϕ_c dependence of these parameters was quite different, they had qualitatively similar x and y dependencies.

[41] If $N_f(\mathbf{x}, \phi_c)$ remained constant, as is the case in many thermodynamic studies, N_f could be combined with the other constants in equation (15) to give

$$S_{Pf,i}(\mathbf{x},\phi_c) = \text{const.}\left[\ln\left(P_i(\mathbf{x},\phi_c)V_f^{5/3}(\mathbf{x},\phi_c)\right)\right] + \text{const.} \quad (16)$$

Then $S_{Pf,i}$ would be a function of $P_iV_f^{5/3}$ alone, so $P_iV_f^{5/3}$ would be conserved between points $\mathbf{x}_1$ and $\mathbf{x}_2$ if the flow was isentropic $[S_{Pf,i}(\mathbf{x}_2, \phi_{c2}) - S_{Pf,i}(\mathbf{x}_1, \phi_{c1}) = 0]$.

[42] Figure 5b provides an additional piece of information that helps to explain why the similarities and differences in this long-term averaged study arose. Equation (14) showed that

$$P_i\ V_f^{5/3} = N_f\ k\ T_iV_f^{2/3} \quad (17)$$

so gradients of $P_iV_f^{5/3}$ and of either $S_{Hf,i}$ or $S_{Pf,i}$ would be dominated by a linear dependence on N_f if N_f varied much more strongly than the energy invariant $T_iV_f^{2/3}$. Figure 5b shows that the ϕ_c dependence of $T_iV_f^{2/3}$ was strong and was directed oppositely to that of N_f, producing qualitative differences between the ϕ_c dependencies of $P_iV_f^{5/3}$ and of $S_{Hf,i}$ or of $S_{Pf,i}$. For example, at $x \sim 20$ R$_E$ the long-term averaged $S_{Hf,i}$ in slow flow regions ($\phi_c = 4$ V) was typically twice as large as in fast flow regions ($\phi_c = 12$ V) even though $P_iV_f^{5/3}$ was typically the same in both regions. However, the y dependence of $T_iV_f^{2/3}$ was very weak and both N_f and $T_iV_f^{2/3}$ increased as one moves out from $x = -10$ R$_E$ to $x = -30$ R$_E$ producing qualitatively similar x and y dependencies of $P_iV_f^{5/3}$ and of $S_{Hf,i}$ or of $S_{Pf,i}$.

[43] An equivalent and possibly simpler way to view the relationship between these parameters is to note that equations (15) and (17) show that $S_{Pf,i}$ depends linearly upon N_f but only weakly or logarithmically upon $T_iV_f^{2/3}/N_f^{2/3}$. The strong similarity between the structures of Figures 4b and 5a emphasized that the x, y and ϕ_c dependencies of $S_{Hf,i}$ could almost completely be explained by the linear dependence on N_f. In contrast, equation (17) shows that $P_iV_f^{5/3}$ depends linearly upon both N_f and $T_iV_f^{2/3}$. Therefore the long-term averaged x, y and ϕ_c dependencies of $P_iV_f^{5/3}$ and of $S_{Hf,i}$ or of $S_{Pf,i}$ will be different if the long-term averaged $T_iV_f^{2/3}$ depends strongly upon x, y or ϕ_c.

[44] Three related physical processes have been proposed that may help explain the long term averages of $P_iV_f^{5/3}$, $S_{Hf,i}$ and $S_{Pf,i}$. One process is that an interchange instability causes low entropy flux tubes or bubbles to move earthward, to accumulate, and therefore to become dominant at small $|x|$ [*Pontius and Wolf*, 1990; *Chen and Wolf*, 1993, 1999; *Sergeev et al.*, 1996; *Birn et al.*, 2009; *Wolf et al.*, 2009]. *Angelopoulos et al.* [1994] showed that the earthward fast flows dominated the earthward transport of plasma, magnetic flux, and energy. Combining this with the observations that fast flow flux tubes had unusually small values of N_f, $S_{Hf,i}$ and $S_{Pf,i}$ provides support for the above suggestion.

[45] Local reconnection, within the $-30 < x < -8$ R_E region studied in this paper, is a related process that would produce an earthward reduction of N_f and therefore of all the parameters being examined here even if the interchange process were not important. It is likely that the fast earthward flows were generated in association with reconnection events either in the local region or farther out in the magnetotail. Many ions are lost from flux tubes and move tailward as plasmoids or flux ropes during any reconnection event, thereby reducing the average N_f near the reconnection location.

[46] The final physical process that has been proposed and that can produce an earthward reduction of N_f, $P_iV_f^{5/3}$, $S_{Hf,i}$ and $S_{Pf,i}$ involves the different drift paths taken by low- and high-energy particles and the resulting mixing of particles from different sources [*Tsyganenko*, 1982; *Spence and Kivelson*, 1993; *Garner et al.*, 2003; *Wang et al.*, 2009; *Lyons et al.*, 2009]. Some combination of these mechanisms is likely to be able to explain the observations [*Wolf et al.*, 2009]. However, it is not clear that a unique combination can be found using long-term averaged studies.

2.4. Average Entropy Per Ion

[47] The substantial x, y and ϕ_c variations of N_f make spatial studies of the plasma sheet more difficult than studies such as the heating or compression of a fixed number of particles in a closed box. An obvious way to eliminate some of these complications is to evaluate either $S_{Hf,i}/N_f$ or $s_{H,i}/n_i$, the average Boltzmann entropy per ion. Unfortunately, these are ratios of pairs of parameters with similar spatial and ϕ_c dependencies (Figures 4b and 5a or Figures 1a and 1b), so uncertainties of the average entropy per ion are relatively large.

[48] The most important feature in Figure 6a is that $(S/Nc_v)_{H,i}$ in the fastest flow regions was larger by 1.7 units at $x = -28$ R_E and by 1.0 unit at $x = -10$ R_E than in slow flow regions. It may be noted that a change of $(S/Nc_v)_{P,i}$ by 1 or 2 units corresponds to a change of $P/n^{5/3}$ by factors of e^1 or e^2. The strong ϕ_c dependence of $(S/Nc_v)_{H,i}$ suggests that a nonadiabatic process heated the average ion and that an irreversible process also may have been involved during the production of fast flows. If the acceleration was associated with reconnection, this implies that something related to the reconnection process was not isentropic. In addition, the ϕ_c dependence shows that heat transfer from fast to slow flow plasmas may take place within the region studied here.

[49] Figure 6b shows $(S/Nc_v)_{P,i}$ for a Maxwellian plasma with the observed $P_i(\mathbf{x})$ and $n_i(\mathbf{x})$. A comparison with Figure 6a shows differences especially between the x and y dependencies of $(S/Nc_v)_{H,i}$ and $(S/Nc_v)_{P,i}$. It will be seen in section 3 that corrections for instrumental and data processing effects change the plot of $(S/Nc_v)_{H,i}$ so that it looks more like that of $(S/Nc_v)_{P,i}$.

[50] Figures 6a and 6b both showed that the average entropy per ion near midnight was ~0.5 unit larger than near the flanks when the flow speed was low, but that there was little y dependence when the flow speed was high. *Borovsky et al.* [1998] and *Johnson and Wing* [2009] previously reported that the average entropy per ion in the plasma sheet increased as midnight was approached. Figure 6 therefore shows that this particular aspect of apparent nonadiabaticity in the plasma sheet is primarily associated with slow flow periods. The observation that the cold dense plasma sheet is more prominent near the flanks than near midnight also may contribute to this y dependence. Finally, a weak earthward increase in the entropy per ion is seen at least during slow flows. The instrumental effects on this gradient are discussed in section 3.

[51] Figure 7a shows the entropy parameter $P_i/n_i^{5/3}$ that is closely related to $(S/Nc_v)_{P,i}$ (equation (6)) and was evaluated using data from many magnetospheric satellites [*Huang et al.*, 1989; *Goertz and Baumjohann*, 1991; *Borovsky et al.*, 1998; *Kaufmann et al.*, 2005; *Birn et al.*, 2006; *Johnson and Wing*, 2009]. A comparison of Figures 6b and 7a shows the expected strong similarities. Differences are produced by the use of linear averages of $P_i/n_i^{5/3}$ in Figure 7a as compared to linear averages of $\ln(P_i/n_i^{5/3})$ in Figure 6b, which corresponds to geometric averages of $P_i/n_i^{5/3}$.

[52] To summarize, the x gradient of $(S/Nc_v)_{H,i}$ was in the same direction as that of $s_{H,i}$ and opposite to that of $S_{Hf,i}$. The y and ϕ_c dependencies of $(S/Nc_v)_{H,i}$, $(S/Nc_v)_{P,i}$ and $P_i/n_i^{5/3}$ were in the opposite sense from the variations in $s_{H,i}$ and $S_{Hf,i}$. The average Boltzmann entropy per particle therefore exhibited spatial and ϕ_c dependencies that differed substantially from those of $s_{H,i}$ and $S_{Hf,i}$ (Table 1). These entropy-per-ion parameters are particularly useful in determining where ions either were nonadiabatically heated or experienced an irreversible process rather than where the average number of particles per unit volume or per unit flux tube was largest.

3. Deviation From Thermodynamic Equilibrium

[53] The difference $\delta(S/Nc_v)_i = (S/Nc_v)_{P,i} - (S/Nc_v)_{H,i}$ is a measure of the deviation from Boltzmann equilibrium (Figure 7b). Several questions have arisen about the physical significance of $\delta(S/Nc_v)_i$ when applied to space plasmas

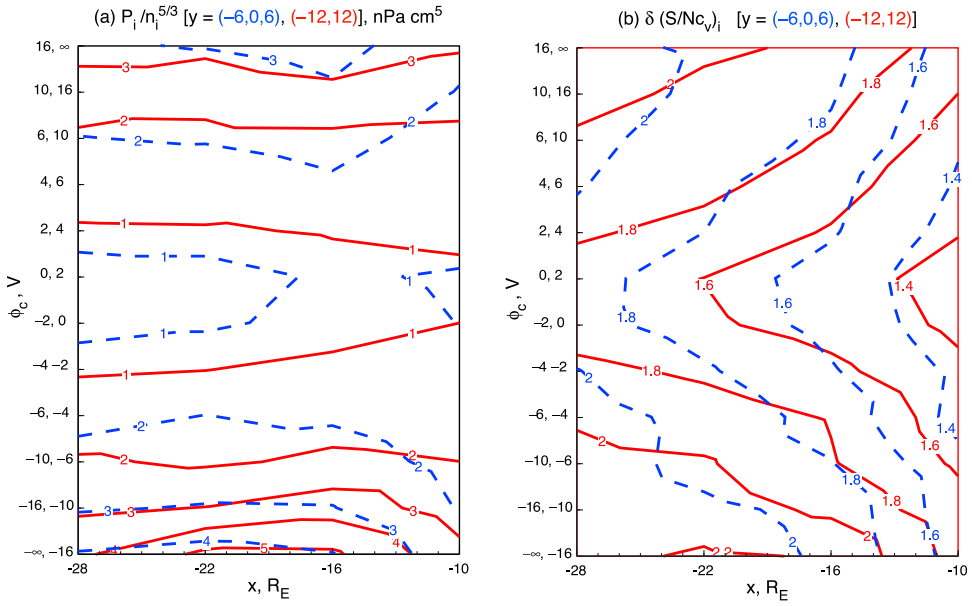

Figure 7. Similar to Figure 1 except showing (a) the average entropy per ion parameter $P_i/n_i^{5/3}$ and (b) a measure of the deviation of the observed plasma from equilibrium $\delta(S/Nc_v)_i = (S/Nc_v)_{P,i} - (S/Nc_v)_{H,i}$.

and about systematic errors associated with the relatively small difference between two calculations of the entropy per ion, each of which depends on the ratio of two fluid parameters with similar structures. Section 3 is intended to examine these questions.

3.1. Sensitivity to Count Rate Cutoffs

[54] It was the sensitivity of $\delta(S/Nc_v)_i$ to the count rate cutoff and the similarity of the shapes of contours of constant R_i (Figure 2a) to $\delta(S/Nc_v)_i$ contours that led to a more detailed examination of the effects of data processing procedures on the fluid parameters. Increasing the cutoff from 80 to 160 did not change the difference between $(S/Nc_v)_{P,i}$ and $(S/Nc_v)_{H,i}$ significantly at $x = -10$ R_E but decreased this difference by 0.07 at $x = -28$ R_E. Increasing the cutoff to 320 counts decreased $\delta(S/Nc_v)_i$ by 0.06 at $x = -10$ R_E and by 0.39 at $x = -28$ R_E. This rather drastic increase in the cutoff would reduce the change in $\delta(S/Nc_v)_i$ between $x = -28$ and $x = -10$ R_E by 0.32, or by more than half the 0.52 change shown in Figure 7b. Both $(S/Nc_v)_{P,i}$ and $(S/Nc_v)_{H,i}$ decreased as the R_i cutoff increased, but $(S/Nc_v)_{P,i}$ decreased more steeply as a result of the elimination of most fast flow data points at $x = -28$ R_E (Figure 2a).

3.2. Model Distribution Functions

[55] We wanted to see how large $\delta(S/Nc_v)_i$ would be in a uniform plasma if $f(\mathbf{v})$ was given by the smooth analytic non-Maxwellian distribution functions that have been used to fit observations in the plasma sheet. The purpose was to see if any $f(\mathbf{v})$was likely to produce $\delta(S/Nc_v)_i$ as large as is shown in Figure 7b. The procedures first were checked by using numerical integration to evaluate H_i (equation (1)) for a standard equilibrium isotropic Maxwellian

$$f(\mathbf{v}) = n\left(\frac{m}{2\pi kT}\right)^{3/2}\exp\left[\frac{-mv^2}{2kT}\right], \tag{18}$$

using this result and equation (5) to evaluate $(S/Nc_v)_{H,i}$, and comparing the result to $(S/Nc_v)_{P,i}$ as determined by equation (6). Parameters typical of those seen at midnight: $n_i = 0.5$ cm^{-3} and $T_i = 4$ keV, gave almost identical results for these two entropy-per-ion expressions, or $\delta(S/Nc_v)_i = 0$, as expected.

[56] An isotropic Lorentzian or kappa distribution function [*Summers and Thorne*, 1991]

$$f(\mathbf{v}) = n \times \left[\frac{m}{2\pi kT\left(\kappa - {}^3\!/_2\right)}\right]^{3/2}\left[\frac{\Gamma(\kappa+1)}{\Gamma\left(\kappa - {}^1\!/_2\right)}\right]\left[1 + \frac{mv^2}{2kT\left(\kappa - {}^3\!/_2\right)}\right]^{-\kappa-1} \tag{19}$$

with the same n_i and T_i then was substituted for the isotropic Maxwellian. *Christon et al.* [1989, 1991] found that the most probable κ values for ions in the plasma sheet were $5 \le \kappa \le 7$. The resulting $\delta(S/Nc_v)_i$ was 0.13, 0.06, 0.03, 0.02, 0.015, and 0.011 when κ was 3, 4, 5, 6, 7 and 8, respectively. The conclusion therefore is that the existence of isotropic κ distributions does not contribute significantly to the magnitude of $\delta(S/Nc_v)_i$ shown in Figure 7b. The physical significance of the observed isotropic κ distributions will be discussed in section 3.5.

[57] Bi-Maxwellian electron and ion distributions

$$f(\mathbf{v}) = n\left(\frac{m}{2\pi kT_\perp}\right)\left(\frac{m}{2\pi kT_\parallel}\right)^{1/2}\exp\left[-\frac{mv_\perp^2}{2kT_\perp} - \frac{mv_\parallel^2}{2kT_\parallel}\right], \tag{20}$$

sometimes with a superimposed bulk flow, also have been seen. A stationary bi-Maxwellian was used to calculate $\delta(S/Nc_v)_i$ with $n_i = 0.5$ cm^{-3} and $T_i = (2T_\perp + T_\parallel)/3 = 4$ keV. The resulting values of $\delta(S/Nc_v)_i$ were 0.1 for $T_\parallel/T_\perp = 3$ and 0.6 for $T_\parallel/T_\perp = 10$. Values as large as those shown in Figure 7b

required $T_{\|}/T_{\perp}$ or $T_{\perp}/T_{\|}$ between 30 and 100. However, the average temperature anisotropy seen near the neutral sheet was much less than 3 [*Kaufmann et al.*, 2005].

[58] Bi-Lorentzian distributions

$$f(\mathbf{v}) = n\left[\frac{m}{2\pi k\left(\kappa - 3/2\right)}\right]^{3/2}\left[\frac{1}{T_{\perp}T_{\|}^{1/2}}\frac{\Gamma(\kappa+1)}{\Gamma\left(\kappa - 1/2\right)}\right]\left[1 + \frac{mv_{\perp}^2}{2kT_{\perp}\left(\kappa - 3/2\right)} + \frac{mv_{\|}^2}{2kT_{\|}\left(\kappa - 3/2\right)}\right]^{-\kappa-1} \tag{21}$$

required temperature anisotropies that were almost as large as those needed for bi-Maxwellians in order to produce the $\delta(S/Nc_v)_i$ magnitudes shown in Figure 7b.

[59] Distribution functions with high energy tails stretched out in only one direction are reasonably common [*Nakamura et al.*, 1991; *Mukai et al.*, 1998; *Ball et al.*, 2005]. A large $|U_i|$ often was produced by an $f(\mathbf{v})$ containing a directionally asymmetric high energy tail or plateau rather than by an $f(\mathbf{v})$ that was isotropic in a frame moving at $\mathbf{U}_i$ relative to the satellite. Calculations therefore were carried out using a bi-Maxwellian multiplied by $(1 + A\cos\psi)$ where ψ is the azimuthal angle around the **B** axis and A is an amplitude factor. These distribution functions typically increased $\delta(S/Nc_v)_i$ by less than 0.2 so still could not create values as large as those shown in Figure 7b.

[60] The conclusion to this point was that none of the smooth distribution functions that were typically used to model the plasma sheet contributed significantly to the calculated $\delta(S/Nc_v)_i$. Then a two-component distribution function consisting of a stationary Maxwellian $f_s(\mathbf{v})$ (equation (18)) plus a Maxwellian beam streaming along the magnetic field direction at a speed U_b

$$f_b(\mathbf{v}) = n_b\left(\frac{m}{2\pi kT_b}\right)^{3/2}\exp\left[-\frac{mv_{\perp}^2}{2kT_b} - \frac{m\left(v_{\|} - U_b\right)^2}{2kT_b}\right] \tag{22}$$

was used. Values of $\delta(S/Nc_v)_i$ as large as those seen in Figure 7b were produced with this two-component $f(\mathbf{v})$ when T_b was very small. For example, using a stationary Maxwellian with $n_i = 0.5$ cm^{-3} and $T_i = 4$ keV plus a beam with $n_b = 0.3$ or 0.5 cm^{-3} and $U_b = 500$ km/s required $T_b =$ 10 to 20 eV or 50 to 100 eV, respectively, to produce $\delta(S/Nc_v)_i = 2$. The full width at half maximum of the velocities of a 20 eV beam moving at 500 km/s extends from 448 km/s (1.05 keV in the satellite frame) to 552 km/s (1.59 keV in the satellite frame), so could be detected. Persistent beams with these very low temperatures were rarely if ever seen near the neutral sheet. However, any spiky structures or box-to-box fluctuations in measured distribution functions will make similar contributions to the calculated $\delta(S/Nc_v)_i$.

[61] As a few examples, *Nakamura et al.* [1991], *Mukai et al.* [1998], and *Nagai et al.* [1998] published measured distribution functions from near the neutral sheet that contained spiky structures that look like multiple beams or holes. Features such as these were expected in regions with few counts per velocity space box. Whenever there is a substantial zero-count region in a measured $f(\mathbf{v})$ there will be an adjacent velocity space region containing boxes with few average counts. In a region containing an average of two counts per box, for example, a box containing one count would frequently be found adjacent to a box containing three counts. This region of $f(\mathbf{v})$ therefore would appear to be very spiky, or to be composed of many adjacent one-box-wide beams or holes. Even in regions with a substantial number of counts per box, statistical fluctuations contribute significantly to the jagged detailed nature of each measured $f(\mathbf{v})$ and therefore to $\delta(S/Nc_v)_i$. The question is how much of the measured $\delta(S/Nc_v)_i$ was produced by instrumental, data processing and statistical effects, and how much was a consequence of real fluctuations in $f(\mathbf{v})$ or of persistent beam-like structures. These issues are addressed for the CPI detectors in section 3.3.

3.3. Simulation Results

[62] The CPI detectors made measurements in 24 energy bands E_k, nine polar angle bands θ_l corresponding to the nine separate detectors, and either 8 or 16 azimuthal sectors ϕ_m about the spin axis. The ion counts measured during one minute in these (E_k, θ_l, ϕ_m) velocity space boxes were used to generate each $f(\mathbf{v})$. The averages usually contained a substantial number of adjacent boxes with no counts at the smallest and largest v. For the 16 azimuthal sector set, which was used in paper 1 and in the present study, penetrating energetic particles produced an average of 0.01 counts per box. The most severe background effects were eliminated by excluding results from any box that contained only one count provided that this box was isolated from others that also contained counts.

[63] Simulations to quantify the statistical effects were carried out by assuming that the actual $f(\mathbf{v})$ was a Maxwellian with a given n_i, T_i and U_i plus a uniform 0.01 count/box background. The integer numbers of counts that would be seen in 1 min sampling periods were generated for each (E_k, θ_l, ϕ_m) box based on Poisson statistics. This procedure was repeated many times to generate a set of simulated 1 min averaged distribution functions that were typical of those that would be measured by the CPI detectors. Each simulated $f(\mathbf{v})$ then was processed using the same procedures that were used with the actual measurements to evaluate simulated fluid parameters such as n_i, H_i, T_i, $(S/Nc_v)_{H,i}$, $(S/Nc_v)_{P,i}$ and $\delta(S/Nc_v)_i$.

[64] As a test, when exact noninteger simulated count rates were retained for each (E_k, θ_l, ϕ_m) box and typical plasma sheet values of n_i, T_i and U_i were input, then the calculated values of n_i, T_i and U_i were almost identical to the input values and $\delta(S/Nc_v)_i$ was essentially zero. This is the result expected for a detector that measures an extremely large number of counts during each determination of $f(\mathbf{v})$.

[65] The actual geometric factors and an integer number of counts in each box then were used to calculate simulated values of the fluid parameters. This study also provided justification for the selection of the 80-count cutoff used in the data processing routine. The simulated values of most parameters were nearly meaningless when fewer than ~30 ions were used to approximate each $f(\mathbf{v})$. The use

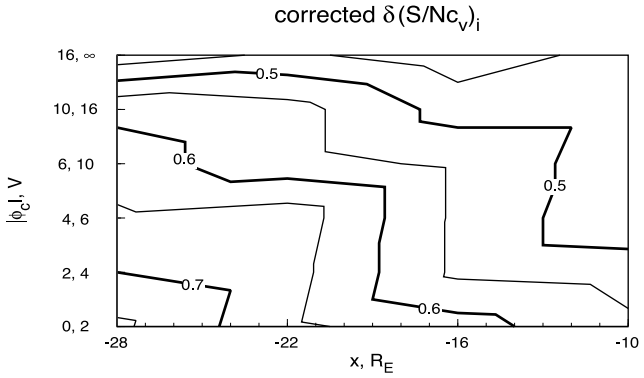

Figure 8. Contour plot of the x and ϕ_c dependencies of $\delta(S/Nc_v)_i$ after correction for instrumental effects attributed to the low number of counts per velocity space box.

of 80 counts for each $f(\mathbf{v})$ produced simulated values of n_i and T_i that fluctuated within 20% of the input parameters. The resulting calculated values of $\delta(S/Nc_v)_i$ were ~1.4. When input parameters were selected that gave an average of 800 counts per determination of $f(\mathbf{v})$, the calculated n_i and T_i were within 10% of the input values and the average calculated $\delta(S/Nc_v)_i$ was ~0.4. The tendency for $\delta(S/Nc_v)_i$ to decrease as the average number of counts increased was expected because $f(\mathbf{v})$ becomes smoother as the average number of counts per (E_k, θ_l, ϕ_m) box increases. Using the 80-count cutoff retained nearly all the data points at the neutral sheet (Figure 2a) and most data throughout the CPS. However, the elimination of low density data points when the cutoff was increased to even 160 counts measurably changed the calculated n_i near $x = -28$ R_E (section 2.2). The $|z| = 5$ R_E cutoff in our modeling region was selected because too many measurements had to be discarded as the lobes were entered when using the 80-count cutoff.

[66] Two other tests were carried out to confirm that it was low count rates and the resulting spiky observed $f(\mathbf{v})$ that were primarily responsible for the generation of $\delta(S/Nc_v)_i$. First, the input U_i was increased to 600 km/s. Detector count rates generally approach zero in boxes near $v = 0$. For a stationary Maxwellian, $f(\mathbf{v})$ peaks at $v = 0$, so the velocity space region of largest $f(\mathbf{v})$ cannot be measured by particle detectors in a stationary plasma. Introducing a large U_i moves this region of maximum $f(\mathbf{v})$ to a velocity region that can be measured, producing (E_k, θ_l, ϕ_m) boxes with substantial numbers of counts. The resulting average calculated $\delta(S/Nc_v)_i$ became smaller, as expected. The second test was to reduce the number of azimuthal sectors from 16 to 8. This cut the total number of (E_k, θ_l, ϕ_m) boxes in half, and therefore doubled the average number of counts per box. This procedure reduced the value of $\delta(S/Nc_v)_i$ by 0.1 to 0.4 for typical CPI count rates.

[67] Next sets of simulations were run using Maxwellians with the actual ϕ_c- and y-averaged values of n_i, T_i and U_i seen in the boxes centered at $x = -28$, -22, -16 and -10 R_E. These runs produced simulated values of $\delta(S/Nc_v)_i$ that were ~2/3 as large as those shown in Figure 7b. The remaining ~1/3 of the measured $\delta(S/Nc_v)_i$ therefore could be attributed to something other than the jagged $f(\mathbf{v})$ produced by low count rates. This remaining corrected $\delta(S/Nc_v)_i$ decreased from 0.7 at $x = -28$ R_E to 0.5 at $x = -10$ R_E. The sense of the x dependence of the corrected $\delta(S/Nc_v)_i$ therefore was the same as that shown in Figure 7b, but the magnitude of the corrected x gradient was smaller.

[68] Finally, a more extended set of simulations was run to determine both the x and ϕ_c dependencies of count rate corrections to $\delta(S/Nc_v)_i$. Since the flow direction was unimportant in evaluations of $\delta(S/Nc_v)_i$ for drifting Maxwellians, measurements of n_i, T_i and U_i for positive and negative ϕ_c were combined and averaged over y to use as inputs to the simulations. Figure 8 shows $\delta(S/Nc_v)_i$ that remained after subtracting these corrections attributed to count rate and data processing effects.

3.4. Conclusions Based on Boltzmann Thermodynamics

[69] The magnitude of the corrected $\delta(S/Nc_v)_i$ still was too large to reasonably be attributed to the presence of the smooth non-Maxwellian distribution functions that have been used to fit plasma sheet ion data. Most of the corrected $\delta(S/Nc_v)_i$ is attributed to the deviation from Boltzmann equilibrium produced by real fluctuations in $f(\mathbf{x}, \mathbf{v}, t)$ because persistent very narrow beams were not common near the neutral sheet. Temporal variations during either one satellite spin period or one fluctuation period can result in a large number of counts in a velocity space box that collected data at one energy during a spin or fluctuation period and a small number of counts in an adjacent box that happened to collect data at a different energy during the next spin or fluctuation period.

[70] Both the original (Figure 7b) and the corrected $\delta(S/Nc_v)_i$ (Figure 8) showed earthward decreases during moderate and slow flow periods. This is the behavior expected if $f(\mathbf{v})$ is either approaching equilibrium or as the fluctuations are decreasing as the plasma moves earthward. However, no significant x dependence was seen during the fastest flow events.

[71] The corrected $\delta(S/Nc_v)_i$ was larger in slow than in fast flows, or in the opposite sense from that shown in Figure 7b. The fastest flows with their low total number of counts (Figure 2a) combined with their high temperatures (Figure 2b) distributed this smaller total number of counts over more (E_k, θ_l, ϕ_m) boxes. This created corrections in the fastest flows that were substantially larger than those associated with the slowest flows, but that also were more uncertain. In addition, *Baumjohann et al.* [1990] noted that flow speeds usually remained continuously above typical fast-flow values for only 5 to 10 s, and rarely remained above these cutoffs for more than 1 min. These strong fluctuations during each 1 min sampling period also contributed to uncertainty in the corrections.

[72] The fact that statistical corrections of the x dependence of $\delta(S/Nc_v)_i$ were modest while corrections of the ϕ_c dependence were larger than the original measurements suggests that the corrected x dependence is more reliable than is the ϕ_c dependence. More accurate measurements of $\delta(S/Nc_v)_i$ would be useful in studies of the evolution of either the shape of $f(\mathbf{v})$ or of the average fluctuation amplitude. Our study showed that it is important to maximize the average number of ion counts per energy angle box that is used to evaluate each measured $f(\mathbf{v})$. Simply averaging many determinations of $\delta(S/Nc_v)_i$ will not reduce this

systematic overestimate if each was evaluated using data containing an inadequate average number of ion counts per energy angle box. For calculations of $\delta(S/Nc_v)_i$ it therefore is desirable to use relatively long data sampling periods and a relatively small number of energy angle boxes in each measured $f(\mathbf{v})$ that is used to evaluate the integral in equation (1). Varying the sampling period also would provide information about fluctuations.

[73] The correction factors discussed here were dominant only when considering the $\delta(S/Nc_v)_i$ parameter. Measurements of H_i, $s_{H,i}$, $S_{Hf,i}$, and $\delta(S/Nc_v)_i$ depended more weakly on the magnitude of fluctuations, while the dependencies of $s_{P,i}$, $S_{Pf,i}$, and $(S/Nc_v)_{P,i}$ were very small. When averaged over ϕ_c and y the corrections to $(S/Nc_v)_{H,i}$ were 1.2 at $x = -28\ R_E$ and 0.9 at $x = -10\ R_E$. These corrections therefore increased the values of $(S/Nc_v)_{H,i}$ shown in Figure 6a by 5% to 6%. This was enough to reduce the difference between the average $(S/Nc_v)_{H,i}$ seen at $x = -28$ R_E and at $x = -10$ R_E from 0.8 (Figure 6a) to 0.5, which is significantly closer to the average 0.3 difference between $(S/Nc_v)_{P,i}$ values seen at these two locations (Figure 6b). The resulting average correction that adds to $-H_i$ (Figure 1a) was only 0.9 at $x = -10$ R_E and 0.7 at $x = -28$ R_E. The final parameter $S_{Hf,i}$ (Figure 5a) was underestimated by an average of ~5% at $x = -10$ R_E and ~6% at $x = -28$ R_E. Since $S_{Hf,i} = -kH_iV_f$ is important when considering the PBI question, it is useful to rewrite this expression as

$$S_{Hf,i} = 3kN_f(S/Nc_v)_{H,i}/2. \tag{23}$$

[74] It is evident that an increase by ~5% of the difference in $(S/Nc_v)_{H,i}$ between $x = -28$ R_E and $x = -10$ R_E represents only a small correction to the factor of 2.8 increase of $S_{Hf,i}$ seen between $x = -10$ R_E and $x = -28$ R_E (Figure 5a). Most of this observed x gradient of $S_{Hf,i}$ was a reflection of a similar gradient in N_f, which was not influenced significantly by those count rate and data processing effects examined here.

3.5. Questions Regarding the Use of Standard Thermodynamics

3.5.1. Restrictions When Using Boltzmann Thermodynamics

[75] A number of restrictions were imposed when developing the laws of standard thermodynamics for equilibrium and for nonequilibrium systems. For example, the Boltzmann H-theorem that describes the evolution of a plasma toward equilibrium was based on effects of two-particle collisions. When viewed over very short time periods this theorem showed that H fluctuated up or down during each collision. However, when viewed macroscopically it statistically was overwhelmingly probable that two-particle collisions would make $H = -s_H/k$ of an isolated gas increasingly more negative until an isotropic Maxwell-Boltzmann equilibrium $f(\mathbf{v})$ was reached.

[76] The basic set of restrictions required to satisfy standard Boltzmann thermodynamics are that extensivity or additivity holds, that any microscopic interactions are short ranged, that the microscopic memory is short ranged or nonexistent, and that the system evolves in a Euclidean-like space-time [*Tsallis*, 1995]. Extensivity of entropy means that if the entropy of one subsystem is $S(A)$ and that of another subsystem is $S(B)$ then the total entropy of the full system would be

$$S(A + B) = S(A) + S(B). \tag{24}$$

[77] The short-ranged restrictions on interactions and on memory permit two-particle collisions but no long-range interactions or correlations. The Euclidean-like requirement means that the system must be continuous and differentiable rather than fractal or coarse grained.

[78] Several of the above restrictions are violated in the Earth's plasma sheet. Space plasmas often are nearly collisionless in the sense that single large angle scattering events involving two charged particles are rare enough to be neglected. The collective behavior of charged particles brought about by many long-range interactions causes much of the momentum transfer in such plasmas [*Ichimaru*, 1973]. Ions in the plasma sheet also are scattered by their chaotic orbital motion near the neutral sheet, where magnetic field lines are strongly curved [*Chen et al.*, 1990; *Burkhart and Chen*, 1992]. This chaotic motion can create an $f_i(\mathbf{x}, \mathbf{v}, t)$ characterized by significant structuring rather than an isotropic Maxwellian. Finally, the evolution of a strongly unstable plasma often stabilizes to a particular instability through the formation of structures such as plateaus rather than to a Maxwellian. For example, plateaus are relatively common in the plasma sheet, as are distributions with high energy tails stretched out in one direction. Quasi-stable distributions composed of distinct hot and cold components also persisted for hours when the interplanetary magnetic field was steadily northward [*Johnson and Wing*, 2009; *Wang et al.*, 2010].

[79] *Kaufmann et al.* [2004a, 2005] used data similar to that described here to conclude that average electrons and ions were scattered or random walked through 90° every minute and that during the fastest flow periods a typical particle undergoes 90° of net scattering as rapidly as once every 10 s. However, these previous studies only considered relaxation of the angular distribution, in particular of the temperature ratio $T_\parallel/T_\perp$, and did not examine relaxation of the energy distribution of $f_a(\mathbf{x}, \mathbf{v}, t)$ toward a steady state.

[80] The Euclidean space-time requirement can be violated if a system is multifractal or coarse grained. In this case Boltzmann entropy may be valid within each grain but would not describe the long-ranged interactions between the grains. One example of this behavior in space plasmas involves the formation of microscopic phase-space structures such as holes and blobs that are generated in an unstable plasma and the subsequent long-ranged interaction of these structures with each other [*Berman et al.*, 1985; *Tetreault*, 1992]. The formation of multiple confined vortices in the LLBL through Kelvin-Helmholtz interactions with the solar wind and subsequent interactions between the resulting vortices provides another example [*Otto and Fairfield*, 2000]. The cascade of energy from large scale to smaller scale turbulent structures followed by the microscopic dissipation of energy at sufficiently small scales is one more example of interactions in a coarse-grained background [*Schekochihin et al.*, 2009].

[81] Another feature of the plasma sheet that violates the assumptions of standard thermodynamics is the presence of strong cross-tail energy- and charge-dependent drifts near the neutral sheet. These drifts make it impossible to define a box or flux tube that contains a fixed group of particles.

3.5.2. Deviations From Boltzmann Thermodynamics

[82] The most thoroughly documented deviation from Boltzmann thermodynamics in the plasma sheet and other space plasmas is the frequent presence of kappa rather than the predicted equilibrium Maxwell-Boltzmann distribution functions [*Christon et al.*, 1989; *Collier*, 1999; *Johnson and Wing*, 2009]. Space plasmas often are considered to be almost collisionless during the time that particles remain in the plasma sheet. If the plasma sheet were completely collisionless then $f_a(\mathbf{x}, \mathbf{v}, t)$ would never evolve along trajectories in phase space. In this event the Vlasov equation would be valid and any $f_a(\mathbf{x}, \mathbf{v}, t)$ that is a function of only the constants of the motion would remain time independent. However, since either Maxwellian or κ distributions usually predominate, some process appears to typically cause plasma sheet particles to evolve toward one of these two forms.

[83] Maxwellians can be attributed to two-particle collisions or to any other interaction that produces a similar collision term in the Boltzmann equation. Several processes have been identified that generate κ distributions. *Collier* [2004] examined the consequence of using Boltzmann's H-function (equation (1)) but with the assumption that the total average energy $\langle \mathcal{H} \rangle$ of a group of particles is not conserved, where $\mathcal{H}$ is the Hamiltonian. He showed that the κ distribution is a natural result if $\langle \ln \mathcal{H} \rangle$, or the geometric average energy per particle is conserved but the linear average $\langle \mathcal{H} \rangle$ is not. Since the plasma sheet is continually driven by the fluctuating solar wind, the assumption that the total energy is not exactly conserved appears to be reasonable. *Collier* [1993] also showed that any process that causes the ions to experience random walk jumps in velocity space, with the jumps governed by a power law, produces $f(\mathbf{v})$ corresponding to a one-dimensional κ function.

[84] Other studies have explored generalized entropy parameters that can be used when the restrictions required by Boltzmann thermodynamics are violated. *Tsallis* [1988, 1995, 1998] proposed a generalized nonextensive entropy that has been used in such situations. The Tsallis entropy can be defined as

$$S_q(p) = -\int p(v)\frac{[p(v)]^{q-1}-1}{q-1}dv \tag{25}$$

where $p(v)$ is the probability distribution of a continuous variable normalized to

$$\int p(v)dv = 1 \tag{26}$$

rather than to n as in equation (3), and q is a nonextensivity index. In practice q represents an additional parameter to adjust that is closely related to the κ index in a κ distribution function [*Silva et al.*, 1998; *Lima et al.*, 2000; *Leubner*, 2002; *Collier*, 2004]. Equations (25) and (26) assume that the distribution is isotropic, so it depends only on the speed of a plasma particle. This same assumption generally has been used when fitting plasma sheet observations to the κ function. The Tsallis entropy reduces to the standard Boltzmann entropy in the limit $q \rightarrow 1$. The nonextensivity results in a deviation from the standard additivity assumption (equation (24)), giving

$$S_q(A+B) = S_q(A) + S_q(B) + (q-1)S_q(A)S_q(B). \tag{27}$$

Physical arguments have been found that show why the formation of κ distributions can be understood based on use of the Tsallis entropy [*Silva et al.*, 1998; *Lima et al.*, 2000; *Milovanov and Zelenyi*, 2000; *Leubner*, 2002].

[85] Maxwellians and κ distributions are similar at small $|\mathbf{v}|$. The principal difference between these two functions is that Maxwellians have exponential high energy tails while the tails of κ distributions follow power laws [*Leubner*, 2002; *Collier*, 2004]. The numerical calculations in section 3.2 showed that the difference between $(S/Nc_v)_{P,i}$ calculated using a Maxwellian and using a $\kappa \sim 6$ distribution was <0.1. Therefore, the corrected $\delta(S/Nc_v)_i$ depended primarily upon the spiky nature of the observations used to evaluate $(S/Nc_v)_{H,i}$. The use of a κ function rather than a Maxwellian to evaluate the equilibrium entropy per ion $(S/Nc_v)_{P,i}$ would produce only a minor change in $\delta(S/Nc_v)_i$. The reason why entropy is so weakly dependent on the shape of the high energy tail of $f(\mathbf{v})$ is because the term added to the normalization integrand (equation (3)) to calculate the entropy (equation (1)) is only logarithmic. In contrast, the terms added to calculate the bulk velocity (equation (7)) and pressure (equation (8)) are linear and quadratic in velocity, respectively. Heat fluxes, which are third velocity moments, are even more sensitive to the shapes of the high energy tails.

[86] The future use of better data sets and incorporation of the data analysis techniques suggested in section 3.4 may be able to improve calculations of $\delta(S/Nc_v)_i$ sufficiently to examine the spatial dependence of deviations of the observed entropy per ion from that predicted by either Maxwellian or κ distributions. For example, section 3.3 showed that the simulated $\delta(S/Nc_v)_i$ calculated using a Maxwellian source $f(\mathbf{v})$ and typical plasma sheet properties decreased from ~1.4 to ~0.4 when the average number of ion counts per data point increased from 80 to 800. A future study therefore could determine if the average form of the plasma $f(\mathbf{v})$ is evolving within the plasma sheet, if plasmas with different $f(\mathbf{v})$ tend to accumulate in different regions of space, or if characteristics of real plasma turbulence exhibit spatial variations.

4. Irreversibility and Summary

4.1. Irreversible Processes During Reconnection

[87] Entropy differences are defined in classical thermodynamics as $dS \geq dQ/T$ where dS is the change in entropy of a closed system, T is the temperature, dQ is the energy transferred to the system as heat, and the equal sign holds for reversible processes. Section 4.1 examines whether irreversible adiabatic ($dQ = 0$) processes can contribute significantly to the observed entropy changes. *Kaufmann and Paterson* [2006] considered a sequence of events involving reconnection that could explain variations of the long-term averaged entropy parameters in the plasma sheet.

For this purpose, the reconnection process was separated into two parts: adiabatic changes associated with the topological reconnection of magnetic field lines and changes produced by nonadiabatic processes.

[88] The adiabatic topological changes involve joining two flux tubes followed by the irreversible mixing and thermalization of the enclosed plasmas [*Johnson and Wing*, 2009]. During flank reconnection, for example, turbulence or instabilities could cause a magnetosheath flux tube with a southward magnetic field to become surrounded by magnetosphere flux tubes with northward magnetic fields. Such a situation can result in a string of multiple reconnection points and multiple plasmoids containing a mixture of the substantially different magnetosheath and magnetosphere plasmas.

[89] In contrast, reconnection involving closed plasma sheet flux tubes consists of joining a northern hemisphere portion of one flux tube with a southern hemisphere portion of the same or a nearby flux tube to produce a new closed flux tube and a detached plasmoid or flux rope. In this case the two initial flux tubes would contain plasmas with similar compositions and other properties so would not significantly change their combined entropy (see Appendix A).

[90] The magnetotail structure with near-Earth and distant neutral lines presented in Figure 3 of *Hones* [1977] illustrates a progression of features that could explain some of the sequence of observations that have been made during substorms. This sequence begins with reconnection of only closed plasma sheet flux tubes to form a plasmoid or flux rope. The plasmoid is released and moves rapidly tailward when all plasma sheet flux tubes have reconnected and lobe field lines begin to reconnect. Figure 10 of *Kaufmann and Paterson* [2006] illustrates the associated abrupt change in the earthward magnetic field tension force in a little more detail. Irreversible processes become more important when the lobe field lines begin to reconnect because, depending on the orientation of the interplanetary magnetic field, there can be substantial differences between the composition, density and temperature of plasmas in the northern and southern lobes. When reconnection does not progress to the lobes a very weak substorm or a pseudobreakup may result. *Tang et al.* [2010] show a detailed example of the differences between pseudobreakups and a substorm expansion as viewed by multiple satellites.

[91] Equation (6) gives the average entropy per ion in a Maxwellian plasma with a temperature T, pressure P and containing N ions within a volume V. However, care must be taken when using this expression to study reconnection. One plasma containing N_1 ions with initial temperature T_{10} and confined to a volume V_{10} will mix with another plasma containing N_2 ions with initial temperature T_{20} and confined to a volume V_{20}. The result of the topological part of reconnection is $N_1 + N_2$ ions in a final volume $V_F = V_{10} + V_{20}$. In standard thermodynamics, two-particle interactions would eventually produce a Maxwellian plasma with a final temperature

$$T_F = \frac{N_1 T_{10} + N_2 T_{20}}{N_1 + N_2}. \tag{28}$$

[92] Using equation (6) to evaluate the sum of the final minus the initial entropies for these plasmas gives the net entropy change ΔS_{Dis} that would be produced if the ions in these two plasmas were distinguishable, e.g., if one was pure H^+ and one was pure O^+ or He^+

$$\Delta S_{Dis} = N_1 k \ln\left[\frac{V_F T_F^{3/2}}{V_{10} T_{10}^{3/2}}\right] + N_2 k \ln\left[\frac{V_F T_F^{3/2}}{V_{20} T_{20}^{3/2}}\right]. \tag{29}$$

[93] Differences between entropies in the initial and final plasma states when the ions are distinguishable and when ions are indistinguishable are discussed in more detail in Appendix A. The importance of several terms in the resulting expressions differ when comparing the reconnection of two closed plasma sheet flux tubes, of two open lobe flux tubes, and of one plasma sheet flux tube with one magnetosheath flux tube. As a numerical example, assume that a plasmoid was formed between two X points from a section of a magnetosheath flux tube with volume $V_{10} = V_0$ containing plasma with density $n_{10} = 10^7$ m^{-3} and initial temperature $T_{10} = 200$ eV that reconnected with a section of a magnetosphere flux tube with volume $V_{20} = V_0$, density $n_{20} = 10^6$ m^{-3} and temperature $T_{20} = 2$ keV. The resulting flux tube or plasmoid would contain $N_F = n_{10}V_0 + n_{20}V_0$ ions with a final temperature $T_F = 360$ eV (equation (28)). Equation (A1) was used to calculate that the change produced in the dimensionless average entropy per ion by the irreversible transfer of heat or the thermalization of these two ion populations with different initial temperatures is $\Delta(S/Nc_v)_A = 0.39$, where the subscript refers to step A in Appendix A. In contrast $\Delta(S/Nc_v)_A = 0$ if two plasma sheet flux tubes with equal initial temperatures $T_{10} = T_{20} = T_F$ reconnected.

[94] Equation (A3) gives the entropy of mixing (step C) when distinguishable groups of ions with the same temperatures and densities mix. If the two plasmas defined above had completely different compositions then equation (A3) would give $\Delta(S/Nc_v)_C = 0.20$. There is no entropy of mixing, so $\Delta(S/Nc_v)_C = 0$, if two plasma sheet flux tubes with identical initial compositions reconnected.

[95] Equations (A2) and (A4) contribute to the entropy increase resulting from the adiabatic topological part of reconnection of two flux tubes if $n_{01} \neq n_{02}$. For the example considered here $\Delta(S/Nc_v)_B = -0.14$ and $\Delta(S/Nc_v)_D = 0.40$, while both terms would be zero if the two mixing plasmas had equal densities.

[96] Figure 6 showed that the entropy per ion in fast flows typically exceeded that in slow flows by ~1.5. No slow flow region was found with average entropies per ion that were comparable to those in fast flows. The numerical estimates showed that although irreversible processes can be important on the dayside, in the cusps and in the flanks, it is unlikely that they will produce such large entropy changes elsewhere in the tail. We conclude that if the high average entropy fast flows were generated in association with the reconnection of closed plasma sheet flux tubes, then they must have gained entropy primarily by heating ($dQ \neq 0$) during a nonadiabatic process such as the interaction of ions with shocks associated with reconnection, kinetic Alfvén waves in the flanks [*Johnson and Cheng*, 1997, 2001] or the turbulent dissipation of flow energy. If it is true that pseudobreakups involve only reconnection of closed flux tubes while substorms also involve lobe reconnection, we conclude that irreversible

mixing of the different plasmas from the northern and southern hemisphere lobes could contribute significant extra entropy gains only during substorms.

4.2. Summary

[97] The ϕ_c, x and limited y dependencies of the long-term averaged entropy density, entropy per unit flux tube, and average entropy per ion were examined. Paper 1 showed that the x and y dependencies of the ion entropy density $s_{H,i}$ were primarily reflections of similar variations of the particle density n_i and that most of the gradients could be attributed to compression as plasma moved earthward. The present study showed that $s_{H,i}$ and n_i also shared similar ϕ_c dependencies, both being much larger in slow than in fast flow regions. The entropy and particle densities showed little y dependence during the fastest flows. It therefore was concluded that whatever process created the BBF events and therefore the bulk of the particle, magnetic field and energy transport [*Angelopoulos et al.*, 1994] operated similarly from midnight to near the flanks. The fact that y dependence was absent only during the fastest flows also showed that the processes that generated these flows were different from those producing the convection seen during other time periods.

[98] The spatial variations of $P_iV_f^{5/3}$ were qualitatively similar to variations of the two closely related entropy per unit flux tube parameters $S_{Hf,i}$ and $S_{Pf,i}$, but the ϕ_c dependencies were not. It was found that the x, y and ϕ_c dependencies of $S_{Hf,i}$ or $S_{Pf,i}$ and $P_iV_f^{5/3}$ would be closely related if $T_iV_f^{2/3}$ was relatively uniform. The spatial gradients of $S_{Hf,i}$ or $S_{Pf,i}$ and $P_iV_f^{5/3}$ were primarily dependent on gradients of N_f, but a modest x gradient of $T_iV_f^{2/3}$ in the same direction as that of N_f also contributed to the x gradient of $P_iV_f^{5/3}$. However, N_f and $T_iV_f^{2/3}$ had strong dependencies on ϕ_c in opposite senses, producing little dependence of $P_iV_f^{5/3}$ on the flow speed even though $S_{Hf,i}$ and $S_{Pf,i}$, because of their close correlation with N_f, had a strong ϕ_c dependence. As a result, fast flows tended to exhibit a low entropy per unit flux tube even though the ϕ_c dependence of $P_iV_f^{5/3}$ was weak.

[99] The three average entropy-per-ion parameters: $(S/Nc_v)_{H,i}$, $(S/Nc_v)_{P,i}$ and $P_i/n_i^{5/3}$ are particularly important because they help to locate where the average ion entropy was changing rather than where the long-term averaged number of particles per unit volume or per unit flux tube was changing. The most important observation was that, in direct contrast to the entropy per unit flux tube, the entropy per ion was largest during fast flows. This is because T_i was very high while N_f was very low in fast flows, producing only weak ϕ_c dependencies of P_i and $P_iV_f^{5/3}$. It was concluded that the generation of fast flows involves some nonadiabatic process, presumably associated with reconnection. Both heat dissipation and irreversible processes can be involved in producing this high average entropy per ion. However, it was concluded that irreversible processes during the reconnection of two previously closed flux tubes do not contribute significantly to the entropy increase. Irreversible processes during the reconnection of two previously open lobe flux tubes or during the reconnection of a plasma sheet flux tube with a magnetosheath flux tube could provide a significant contribution.

[100] The parameter $\delta(S/Nc_v)_i$ was calculated for use as a measure of the deviation of the average ion plasma from equilibrium. Questions concerning the use of standard Boltzmann thermodynamics in the plasma sheet were examined. It was seen that deviations from Boltzmann thermodynamics can result in the generation of a kappa rather than a Maxwellian $f(\mathbf{v})$. However, simulations that were carried out showed that it was turbulence and the statistical spikiness in each measured $f(\mathbf{v})$ produced by the limited number of counts in energy angle boxes rather than the shapes of the smooth fitting functions that contributed most to $\delta(S/Nc_v)_i$. Corrections to remove the effects of statistical spikiness modified $(S/Nc_v)_{H,i}$ to more nearly equal $(S/Nc_v)_{P,i}$. Therefore $(S/Nc_v)_{P,i}$ appears to be a better measure of the average entropy per ion than is the uncorrected $(S/Nc_v)_{H,i}$. When the statistical effects were removed, it was concluded that the remaining corrected $\delta(S/Nc_v)_i$ was associated more with real fluctuations than with the deviation of the smoothed structure of $f(\mathbf{v})$ from a Maxwellian. In slow and moderate flow regions $\delta(S/Nc_v)_i$ was smaller at $x = -10$ R_E than at $x = -28$ R_E. No x dependence could be found during the fastest flows. It also appeared that the corrected $\delta(S/Nc_v)_i$ was smaller in fast than in slow flows.

Appendix A

[101] Appendix A examines some effects of reconnection on the average entropy per ion in Maxwellian plasmas. Reconnection events can be associated with irreversible processes, in which case the expression $dS > dQ/T$ must be used. Entropy is similar to parameters such as density and pressure in that it depends only upon the current state of the plasma rather than on how it arrived at that state. When an irreversible process is involved, the entropy change is calculated by following any sequence of reversible processes, for which $dS = dQ/T$, that could bring the plasma from its initial to its final state. The steps described here therefore are not intended to represent a sequence of processes that took place during reconnection, but were picked to provide a way to calculate the net entropy change that took place.

[102] Just before two flux tubes reconnect, the pieces that will merge to form plasmoids, flux ropes or new flux tubes contain N_1 and N_2 ions at temperatures T_{10} and T_{20} that are confined to the volumes V_{10} and V_{20}. The ions are assumed to be ideal monatomic gases with Maxwellian distribution functions so that $PV = NkT$. The first reversible step (step A) is to slowly transfer heat dQ from a reservoir at the final temperature T_F to one ion plasma at a constant volume and to transfer the same dQ from the other plasma to the reservoir so that both plasmas reach the same final temperature (equation (28)). This temperature will remain fixed throughout the remaining steps. The properties of the plasma after step A are $V_{1A} = V_{10}$, $V_{2A} = V_{20}$, $n_{1A} = N_1/V_{10}$, $n_{2A} = N_2/V_{20}$, $T_{1A} = T_{2A} = T_F$, $P_{1A} = N_1kT_F/V_{10}$ and $P_{2A} = N_2kT_F/V_{20}$. The entropy change for reversible constant volume heating or cooling of an ideal monatomic gas from an initial T_I to a final T_F is $\Delta S = (3/2)Nk \ln(T_F/T_I)$, so

$$\Delta S_A = (3/2)N_1k \ln(T_F/T_{10}) + (3/2)N_2k \ln(T_F/T_{20}). \quad \text{(A1)}$$

[103] During step B only plasma 2 will be compressed or expanded isothermally until $P_{2B} = P_{1A} = N_1kT_F/V_{10} = P_{1B}$. The entropy change for reversible isothermal compression

or expansion from an initial V_I to a final V_F is $\Delta S = Nk \ln (V_F/V_I)$. No change takes place in plasma 1 parameters during step B and the altered plasma 2 parameters become $V_{2B} = N_2V_{10}/N_1$ and $n_{2B} = N_1/V_{10}$. The entropy change during this step is

$$\Delta S_B = N_2 k \ln[(N_2V_{10})/(N_1V_{20})]. \quad \text{(A2)}$$

[104] At this point the two plasmas have the same temperatures, pressures and densities. Step C is to simply connect the two flux tubes so the plasmas freely mix into the combined volume $V_C = V_{1B} + V_{2B} = V_{10}(N_1 + N_2)/N_1$. The remaining parameters are $n_{1C} = N_1/V_C$, $n_{2C} = N_2/V_C$, $P_{1C} = N_1kT_F/[V_{10}(N_1 + N_2)/N_1]$ and $P_{2C} = N_2kT_F/[V_{10}(N_1 + N_2)/N_1]$, where P_{1C} and P_{2C} are now the partial pressures of the N_1 and N_2 ions in the combined volume. If ions from the two initial flux tubes were distinguishable, e.g., one flux tube initially contained only H^+ and the other initially contained only O^+ or He^+, then mixing of these two plasmas would be irreversible and

$$\Delta S_C = N_1 k \ln[(N_1 + N_2)/N_1] + N_2 k \ln[(N_1 + N_2)/N_2], \quad \text{(A3)}$$

which is called the entropy of mixing. However, if the two groups of ions were indistinguishable, then mixing the ion groups with the same T, P, and n would result in $\Delta S_C = 0$.

[105] Finally the entire volume V_C of the mixed ion plasma is isothermally compressed or expanded until it reaches the desired final value $V_D = V_{10} + V_{20} = V_F$. The other final parameters are $n_{1D} = N_1/V_F$, $n_{2D} = N_2/V_F$, $P_{1D} = N_1kT_F/V_F = P_{1F}$ and $P_{2D} = N_2kT_F/V_F = P_{2F}$, where P_{1F} and P_{2F} are the final partial pressures and $P_F = P_{1F} + P_{2F}$ is the final total pressure. The entropy change associated with this last step is

$$\Delta S_D = (N_1 + N_2)k \ln\left[\left(\frac{N_1}{N_1 + N_2}\right)\left(1 + \frac{V_{20}}{V_{10}}\right)\right] \quad \text{(A4)}$$

[106] The sum $\Delta S_A + \Delta S_B + \Delta S_C + \Delta S_D$ for the mixing of distinguishable plasmas is equal to ΔS_{Dis} (equation (29)) that was derived directly from equation (6). The sum $\Delta S_{Ind} = \Delta S_A + \Delta S_B + \Delta S_D$ that does not include the entropy of mixing is the change experienced when the two flux tubes that were connected contained indistinguishable ion plasmas. This total indistinguishable ion plasma entropy change is

$$\Delta S_{Ind} = N_1 k \ln\left[\frac{V_F T_F^{3/2} N_1}{V_{10} T_{10}^{3/2}(N_1 + N_2)}\right] + N_2 k \ln\left[\frac{V_F T_F^{3/2} N_2}{V_{20} T_{20}^{3/2}(N_1 + N_2)}\right]. \quad \text{(A5)}$$

[107] **Acknowledgments.** This material is based upon work at the University of New Hampshire that was supported by the National Science Foundation under grant ATM-0741791. The National Aeronautics and Space Administration supported research at Hampton University under grant NAG5-11485. The authors would like to thank L. A. Frank, who developed the Geotail Comprehensive Plasma Instrumentation and was instrumental in initiating this series of studies, T. Nagai, who supplied the suitably averaged Geotail magnetic field measurements, and R. A. Wolf for constructive suggestions.

[108] Masaki Fujimoto thanks the reviewers for their assistance in evaluating this paper.

References

Angelopoulos, V., C. F. Kennel, F. V. Coroniti, R. Pellat, M. G. Kivelson, R. J. Walker, C. T. Russell, W. Baumjohann, W. C. Feldman, and J. T. Gosling (1994), Statistical characteristics of bursty bulk flow events, *J. Geophys. Res.*, *99*, 21,257–21,280, doi:10.1029/94JA01263.

Angelopoulos, V., et al. (1996), Multipoint analysis of a bursty bulk flow event on April 11, 1985, *J. Geophys. Res.*, *101*, 4967–4989, doi:10.1029/95JA02722.

Ball, B. M., R. L. Kaufmann, W. R. Paterson, and L. A. Frank (2005), Non-adiabatic orbit features in ion distribution functions of fast flow magnetotail configurations, *J. Geophys. Res.*, *110*, A04208, doi:10.1029/2004JA010676.

Baumjohann, W., G. Paschmann, and H. Lühr (1990), Characteristics of high-speed ion flows in the plasma sheet, *J. Geophys. Res.*, *95*, 3801–3809, doi:10.1029/JA095iA04p03801.

Berman, R. H., D. J. Tetreault, and T. H. Dupree (1985), Simulation of phase space hole growth and the development of intermittent plasma turbulence, *Phys. Fluids*, *28*, 155–176, doi:10.1063/1.865176.

Birn, J., M. Hesse, and K. Schindler (2006), On the role of entropy conservation and entropy loss governing substorm phases, paper presented at Eighth International Conference on Substorms, Univ. of Calgary, Banff, Canada.

Birn, J., M. Hesse, K. Schindler, and S. Zaharia (2009), Role of entropy in magnetotail dynamics, *J. Geophys. Res.*, *114*, A00D03, doi:10.1029/2008JA014015.

Birn, J., R. Nakamura, E. V. Panov, and M. Hesse (2011), Bursty bulk flows and dipolarization in MHD simulations of magnetotail reconnection, *J. Geophys. Res.*, *116*, A01210, doi:10.1029/2010JA016083.

Borovsky, J. E., M. F. Thomsen, R. C. Elphic, T. E. Cayton, and D. J. McComas (1998), The transport of plasma sheet material from the distant tail to geosynchronous orbit, *J. Geophys. Res.*, *103*, 20,297–20,331, doi:10.1029/97JA03144.

Burkhart, G. R., and J. Chen (1992), Chaotic scattering of pitch angles in the current sheet of the magnetotail, *J. Geophys. Res.*, *97*, 6479–6491, doi:10.1029/91JA03020.

Chen, C. X., and R. A. Wolf (1993), Interpretation of high-speed flows in the plasma sheet, *J. Geophys. Res.*, *98*, 21,409–21,419, doi:10.1029/93JA02080.

Chen, C. X., and R. A. Wolf (1999), Theory of thin-filament motion in Earth's magnetotail and its application to bursty bulk flows, *J. Geophys. Res.*, *104*, 14,613–14,626, doi:10.1029/1999JA900005.

Chen, J., G. R. Burkhart, and C. Y. Huang (1990), Observational signatures of nonlinear magnetotail particle dynamics, *Geophys. Res. Lett.*, *17*, 2237–2240, doi:10.1029/GL017i012p02237.

Christon, S. P., D. J. Williams, D. G. Mitchell, L. A. Frank, and C. Y. Huang (1989), Spectral characteristics of plasma sheet ion and electron populations during undisturbed geomagnetic conditions, *J. Geophys. Res.*, *94*, 13,409–13,424, doi:10.1029/JA094iA10p13409.

Christon, S. P., D. J. Williams, D. G. Mitchell, C. Y. Huang, and L. A. Frank (1991), Spectral characteristics of plasma sheet ion and electron populations during disturbed geomagnetic conditions, *J. Geophys. Res.*, *96*, 1–22, doi:10.1029/90JA01633.

Collier, M. R. (1993), On generating kappa-like distribution functions using velocity space Lévy flights, *Geophys. Res. Lett.*, *20*, 1531–1534, doi:10.1029/93GL01702.

Collier, M. R. (1999), Evolution of kappa distributions under velocity space diffusion: A model for the observed relationship between their spectral parameters, *J. Geophys. Res.*, *104*, 28,559–28,564, doi:10.1029/1999JA900355.

Collier, M. R. (2004), Are magnetospheric suprathermal particle distributions (κ functions) inconsistent with maximum entropy considerations?, *Adv. Space Res.*, *33*, 2108–2112, doi:10.1016/j.asr.2003.05.039.

Erickson, G. M., and R. A. Wolf (1980), Is steady convection possible in the Earth's magnetotail?, *Geophys. Res. Lett.*, *7*, 897–900, doi:10.1029/GL007i011p00897.

Frank, L. A., K. L. Ackerson, W. R. Paterson, J. A. Lee, M. R. English, and G. L. Pickett (1994), The comprehensive plasma instrumentation (CPI) for the Geotail spacecraft, *J. Geomagn. Geoelectr.*, *46*, 23–37, doi:10.5636/jgg.46.23.

Fujimoto, M., T. Terasawa, T. Mukai, Y. Saito, T. Yamamoto, and S. Kokubun (1998), Plasma entry from the flanks of the near-Earth magnetotail: Geotail observations, *J. Geophys. Res.*, *103*, 4391–4408, doi:10.1029/97JA03340.

Garner, T. W., R. A. Wolf, R. W. Spiro, M. F. Thomsen, and H. Korth (2003), Pressure balance inconsistency exhibited in a statistical model of magnetospheric plasma, *J. Geophys. Res.*, *108*(A8), 1331, doi:10.1029/2003JA009877.

Goertz, C. K., and W. Baumjohann (1991), On the thermodynamics of the plasma sheet, *J. Geophys. Res.*, *96*, 20,991–20,998, doi:10.1029/91JA02128.

Hones, E. W., Jr. (1977), Substorm processes in the magnetotail: Comments on "On hot tenuous plasmas, fireballs, and boundary layers in the Earth's magnetotail" by L. A. Frank, K. L. Ackerson, and R. P. Lepping, *J. Geophys. Res.*, *82*, 5633–5640, doi:10.1029/JA082i035p05633.

Huang, C. Y., C. K. Goertz, L. A. Frank, and G. Rostoker (1989), Observational determination of the adiabatic index in the quiet time plasma sheet, *Geophys. Res. Lett.*, *16*, 563–566, doi:10.1029/GL016i006p00563.

Huang, K. (1963), *Statistical Mechanics*, John Wiley, New York.

Ichimaru, S. (1973), *Basic Principles of Plasma Physics: A Statistical Approach*, Benjamin, Reading, Mass.

Johnson, J. R., and C. Z. Cheng (1997), Kinetic Alfvén waves and plasma transport at the magnetopause, *Geophys. Res. Lett.*, *24*, 1423–1426, doi:10.1029/97GL01333.

Johnson, J. R., and C. Z. Cheng (2001), Stochastic ion heating at the magnetopause due to kinetic Alfvén waves, *Geophys. Res. Lett.*, *28*, 4421–4424, doi:10.1029/2001GL013509.

Johnson, J. R., and S. Wing (2009), Northward interplanetary magnetic field plasma sheet entropies, *J. Geophys. Res.*, *114*, A00D08, doi:10.1029/2008JA014017.

Kaufmann, R. L., and W. R. Paterson (2006), Magnetic flux and particle transport in the plasma sheet, *J. Geophys. Res.*, *111*, A10214, doi:10.1029/2006JA011734.

Kaufmann, R. L., and W. R. Paterson (2009), Boltzmann *H* function and entropy in the plasma sheet, *J. Geophys. Res.*, *114*, A00D04, doi:10.1029/2008JA014030.

Kaufmann, R. L., B. M. Ball, W. R. Paterson, and L. A. Frank (2001), Plasma sheet thickness and electric currents, *J. Geophys. Res.*, *106*, 6179–6193, doi:10.1029/2000JA000284.

Kaufmann, R. L., C. Lu, W. R. Paterson, and L. A. Frank (2002), Three-dimensional analyses of electric currents and pressure anisotropies in the plasma sheet, *J. Geophys. Res.*, *107*(A7), 1103, doi:10.1029/2001JA000288.

Kaufmann, R. L., W. R. Paterson, and L. A. Frank (2004a), Magnetization of the plasma sheet, *J. Geophys. Res.*, *109*, A09212, doi:10.1029/2003JA010148.

Kaufmann, R. L., W. R. Paterson, and L. A. Frank (2004b), Pressure, volume, density relationships in the plasma sheet, *J. Geophys. Res.*, *109*, A08204, doi:10.1029/2003JA010317.

Kaufmann, R. L., W. R. Paterson, and L. A. Frank (2005), Relationships between the ion flow speed, magnetic flux transport rate, and other plasma sheet parameters, *J. Geophys. Res.*, *110*, A09216, doi:10.1029/2005JA011068.

Kokubun, S., T. Yamamoto, M. H. Acuna, K. Hayashi, K. Shiokawa, and H. Kawano (1994), The Geotail magnetic field experiment, *J. Geomagn. Geoelectr.*, *46*, 7–21, doi:10.5636/jgg.46.7.

Krall, N. A., and A. W. Trivelpiece (1973), *Principles of Plasma Physics*, McGraw-Hill, New York.

Larson, D. J., and R. L. Kaufmann (1996), Structure of the magnetotail current sheet, *J. Geophys. Res.*, *101*, 21,447–21,461.

Leubner, M. P. (2002), A nonextensive entropy approach to kappa-distributions, *Astrophys. Space Sci.*, *282*, 573–579, doi:10.1023/A:1020990413487.

Lima, J. A. S., R. Silva Jr., and J. Santos (2000), Plasma oscillations and nonextensive statistics, *Phys. Rev. E*, *61*, 3260–3263, doi:10.1103/PhysRevE.61.3260.

Lyons, L. R., C.-P. Wang, M. Gkioulidou, and S. Zou (2009), Connections between plasma sheet transport, region 2 currents, and entropy changes associated with convection, steady magnetospheric convection periods, and substorms, *J. Geophys. Res.*, *114*, A00D01, doi:10.1029/2008JA013743.

Milovanov, A. V., and L. M. Zelenyi (2000), Functional background of the Tsallis entropy: "Coarse-grained" systems and "kappa" distribution functions, *Nonlinear Processes Geophys.*, *7*, 211–221, doi:10.5194/npg-7-211-2000.

Mukai, T., T. Yamamoto, and S. Machida (1998), *Dynamics and Kinetic Properties of Plasmoids and Flux Ropes: Geotail Observations*, *Geophys. Monogr. Ser.*, vol. 105, pp. 117–137, AGU, Washington, D. C.

Nagai, T., M. Fujimoto, Y. Saito, S. Machida, T. Terasawa, R. Nakamura, T. Yamamoto, T. Mukai, A. Nishida, and S. Kokubun (1998), Structure and dynamics of magnetic reconnection for substorm onsets with Geotail observations, *J. Geophys. Res.*, *103*, 4419–4440, doi:10.1029/97JA02190.

Nagata, D., S. Machida, S. Ohtani, Y. Saito, and T. Mukai (2008), Solar wind control of plasma number density in the near-Earth plasma sheet: Three-dimensional structure, *Ann. Geophys.*, *26*, 4031–4049, doi:10.5194/angeo-26-4031-2008.

Nakamura, M., G. Paschmann, W. Baumjohann, and N. Sckopke (1991), Ion distributions and flows near the neutral sheet, *J. Geophys. Res.*, *96*, 5631–5649, doi:10.1029/90JA02495.

Otto, A., and D. H. Fairfield (2000), Kelvin-Helmholtz instability at the magnetotail boundary: MHD simulation and comparison with Geotail observations, *J. Geophys. Res.*, *105*, 21,175–21,190, doi:10.1029/1999JA000312.

Pontius, D. H., and R. A. Wolf (1990), Transient flux tubes in the terrestrial magnetosphere, *Geophys. Res. Lett.*, *17*, 49–52, doi:10.1029/GL017i001p00049.

Rossi, B., and S. Olbert (1970), *Introduction to the Physics of Space*, McGraw-Hill, New York.

Schekochihin, A. A., S. C. Cowley, W. Dorland, G. W. Hammett, G. G. Howes, E. Quataert, and T. Tatsuno (2009), Astrophysical gyrokinetics: Kinetic and fluid turbulent cascades in magnetized weakly collisional plasmas, *Astrophys. J. Suppl. Ser.*, *182*, 310–377, doi:10.1088/0067-0049/182/1/310.

Schödel, R., R. Nakamura, W. Baumjohann, and T. Mukai (2001), Rapid flux transport and plasma sheet reconfiguration, *J. Geophys. Res.*, *106*, 8381–8390, doi:10.1029/2000JA900159.

Sckopke, N., G. Paschmann, G. Haerendel, B. U. Ö. Sonnerup, S. J. Bame, T. G. Forbes, E. W. Hones Jr., and C. T. Russell (1981), Structure of the low-latitude boundary layer, *J. Geophys. Res.*, *86*, 2099–2110, doi:10.1029/JA086iA04p02099.

Sergeev, V. A., V. Angelopoulos, J. T. Gosling, C. A. Cattell, and C. T. Russell (1996), Detection of localized, plasma-depleted flux tubes or bubbles in the midtail plasma sheet, *J. Geophys. Res.*, *101*, 10,817–10,826, doi:10.1029/96JA00460.

Silva, R., Jr., A. R. Plastino, and J. A. S. Lima (1998), A Maxwellian path to the q-extensive velocity distribution function, *Phys. Lett. A*, *249*, 401–408, doi:10.1016/S0375-9601(98)00710-5.

Speiser, T. W. (1965), Particle trajectories in model current sheets: 1. Analytic solutions, *J. Geophys. Res.*, *70*, 4219–4226, doi:10.1029/JZ070i017p04219.

Spence, H. E., and M. G. Kivelson (1993), Contributions of the low-latitude boundary layer to the finite width magnetotail convection model, *J. Geophys. Res.*, *98*, 15,487–15,496, doi:10.1029/93JA01531.

Summers, D., and R. M. Thorne (1991), The modified plasma dispersion function, *Phys. Fluids B*, *3*, 1835–1847, doi:10.1063/1.859653.

Tang, C. L., V. Angelopoulos, A. Runov, C. T. Russell, H. Frey, K. H. Glassmeier, K. H. Fornacon, and Z. Y. Li (2010), Precursor activation and substorm expansion associated with observations of a dipolarization front by Thermal Imaging System (THEMIS), *J. Geophys. Res.*, *115*, A07215, doi:10.1029/2009JA014879.

Tetreault, D. (1992), Turbulent relaxation of magnetic fields: 1. Coarse-grained dissipation and reconnection, *J. Geophys. Res.*, *97*, 8531–8540, doi:10.1029/92JA00309.

Tsallis, C. (1988), Possible generalization of Boltzmann-Gibbs statistics, *J. Stat. Phys.*, *52*, 479–487, doi:10.1007/BF01016429.

Tsallis, C. (1995), Non-extensive thermostatistics: Brief review and comments, *Physica A*, *221*, 277–290, doi:10.1016/0378-4371(95)00236-Z.

Tsallis, C. (1998), Generalized entropy-based criterion for consistent testing, *Phys. Rev. E*, *58*, 1442–1445, doi:10.1103/PhysRevE.58.1442.

Tsyganenko, N. A. (1982), On the convective mechanism for formation of the plasma sheet in the magnetospheric tail, *Planet. Space Sci.*, *30*, 1007–1012, doi:10.1016/0032-0633(82)90150-7.

Tsyganenko, N. A. (1989), A magnetospheric magnetic field model with a warped tail current sheet, *Planet. Space Sci.*, *37*, 5–20, doi:10.1016/0032-0633(89)90066-4.

Tsyganenko, N. A. (1995), Modeling the Earth's magnetospheric magnetic field confined within a realistic magnetopause, *J. Geophys. Res.*, *100*, 5599–5612, doi:10.1029/94JA03193.

Tsyganenko, N. A. (1996), Effects of the solar wind conditions on the global magnetospheric configuration as deduced from data-based field models, in *Proceedings of the ICS-3 Conference on Substorms*, *Eur. Space Agency Spec. Publ.*, *ESA SP-389*, 181–185.

Wang, C.-P., L. R. Lyons, J. M. Weygand, T. Nagai, and R. W. McEntire (2006), Equatorial distributions of the plasma sheet ions, their electric and magnetic drifts, and magnetic fields under different interplanetary magnetic field Bz conditions, *J. Geophys. Res.*, *111*, A04215, doi:10.1029/2005JA011545.

Wang, C.-P., L. R. Lyons, R. A. Wolf, T. Nagai, J. M. Weygand, and A. T. Y. Lui (2009), Plasma sheet $PV^{5/3}$ and nV and associated plasma and energy transport for different convection strengths and *AE* levels, *J. Geophys. Res.*, *114*, A00D02, doi:10.1029/2008JA013849.

Wang, C.-P., L. R. Lyons, T. Nagai, J. M. Weygand, and A. T. Y. Lui (2010), Evolution of plasma sheet particle content under different interplanetary magnetic field conditions, *J. Geophys. Res.*, *115*, A06210, doi:10.1029/2009JA015028.

Wolf, R. A. (1983), The quasi-static (slow-flow) region of the magnetosphere, in *Solar-Terrestrial Physics*, edited by R. L. Carovillano and J. M. Forbes, pp. 303–368, D. Reidel, Dordrecht, Netherlands.

Wolf, R. A., Y. Wan, X. Xing, J.-C. Zhang, and S. Sazykin (2009), Entropy and plasma sheet transport, *J. Geophys. Res.*, *114*, A00D05, doi:10.1029/2009JA014044.

Zhang, J.-C., R. A. Wolf, R. W. Spiro, G. M. Erickson, S. Sazykin, F. R. Toffoletto, and J. Yang (2009), Rice convection model simulation of the substorm-associated injection of an observed plasma bubble into the inner magnetosphere: 2. Simulation results, *J. Geophys. Res.*, *114*, A08219, doi:10.1029/2009JA014131.

R. L. Kaufmann, Department of Physics, University of New Hampshire, Durham, NH 03824, USA. (dick.kaufmann@unh.edu)

W. R. Paterson, Department of Atmospheric and Planetary Sciences, Hampton University, Hampton, VA 23668, USA.